2003

A numerical simulation on Japan/East Sea (JES) thermohaline structure and circulation

Fan, C.W.

Chu, P.C., S.H. Lu, C.W. Fan

Advances in Coastal Modeling
edited by C. Lakhan

Chapter 16

A Numerical Simulation of Japan/East Sea (JES) Thermohaline Structure and Circulation

Peter C. Chu [a], Shihua Lu [a], Chenwu Fan [a] and Chang S. Kim [b]

[a]Department of Oceanography, Naval Postgraduate School, Monterey, CA 93943
[b]Korea Ocean R&D Institute, Ansan 425–170, South Korea

1. INTRODUCTION

The Japan Sea, known as the East Sea in Korea, has a steep bottom topography (Fig. 1) that makes it a unique semi-enclosed ocean basin overlaid by a pronounced monsoon surface wind. The Japan/East Sea, hereafter referred to as JES, covers an area of 10^6 km^2. It has a maximum depth in excess of 3,700 m, and is isolated from open oceans except for small (narrow and shallow) straits, which connect the JES with the North Pacific through the Korea/Tsushima and Tsugaru Straits and

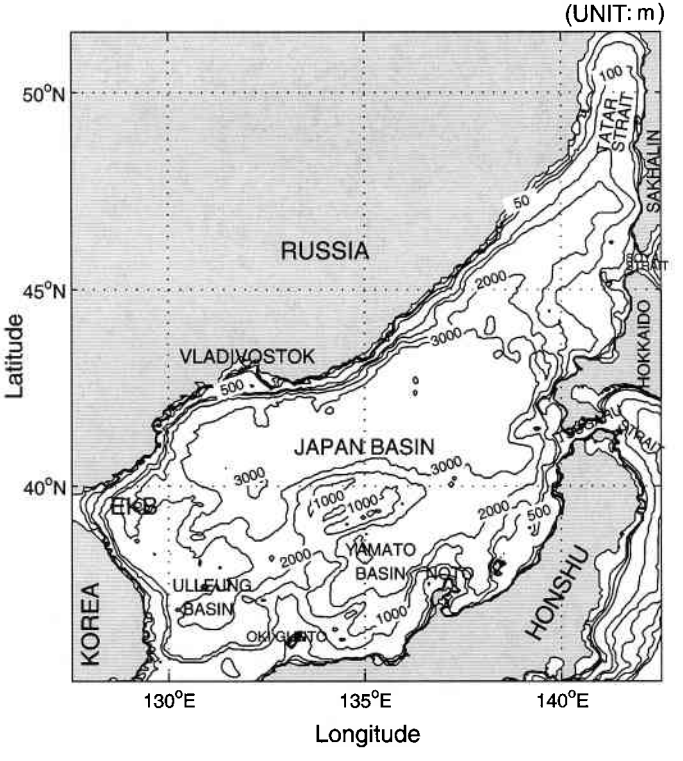

Figure 1. The bottom topography (m) of the Japan/East Sea (JES).

with the Okhotsk Sea through the Soya and Tatar Straits. The JES contains three major basins called the Japan Basin (JB), Ulleung/Tsushima Basin (UTB), and Yamato Basin (YB), and has a high central plateau called the Yamato Rise (YR). The JES has great scientific interest as a miniature prototype ocean. Its basin-wide circulation pattern, boundary currents, Subpolar Front (SPF), mesoscale eddy activities and deep water formation are similar to those in a large ocean.

The JES thermohaline structure and general circulation have been investigated for several decades. The Tsushima Warm Current (TWC), dominating the surface layer, flows in from the Tsushima Strait, and carries warm water from the south up to 40°N where a polar front forms (Seung and Yoon, 1995). Most of the nearly homogeneous water in the deep part of the basin is called the Japan Sea Proper Water (Moriyasu, 1972), and is of low temperature and low salinity. Above the Proper Water, warm and saline water flows in through the Tsushima Strait, transports northeastward, and flows out through the Tsugaru and Soya Strait.

The TWC separates north of 35°N into western and eastern channels (Uda, 1934; Kawabe, 1982a; 1982b; Hase et al., 1999; Senjyu, 1999). The flow through the western channel closely follows the Korean coast [called the East Korean Warm Current (EKWC)] until it bifurcates into two branches near 37°N. The eastern branch follows the SPF to the western coast of Hokkaido Island, and the western branch moves northward and forms a cyclonic eddy at the Eastern Korean Bay (EKB). The EKWC meets the southward coastal current, the North Korean Cold Current (NKCC), at about 38°N with some seasonal meridional migration. After separation from the coast, the EKWC and the NKCC converge and form a strong front (i.e., SPF) that stretches in a west-east direction across the basin. The NKCC makes a cyclonic recirculation gyre in the north but most of the EKWC flows out through the outlets (Uda, 1934). The formation of the NKCC and the separation of the EKWC are due to a local forcing by wind and buoyancy flux (Seung, 1992). Large meanders develop along the front and are associated with warm and cold eddies.

Seasonal variability of the JES thermohaline structure has been studied by many investigators (Gong and Park, 1969; Isoda et al., 1991; Isoda and Saitoh, 1993; Maizuru Marine Observatory, 1997) using limited data sets. For example, after analyzing satellite infrared (IR) images and routine hydrographic survey data (by the Korea Fisheries Research and Development Agency) for the western part of the JES in the winter and the spring 1987, Isoda and Saitoh (1993) found that a small meander of a thermal front originates from the Korean/Tsushima Strait near the Korean coast and gradually grows into an isolated warm eddy with a horizontal scale of 100 km. The warm eddy moves slowly northward from spring to summer.

Although the seasonal thermal variability on 150 m depth is weaker than on the surface, SPF still occurs at around 40°N all the time throughout the year and is located at almost the same location as at the surface. It divides the water masses with different characteristics. North of the SPF, temperature is uniformly cold (1°– 3°C) throughout the year. South of the SPF, temperature changes from 5°C to 9°C. The SPF meandering at 131°E, 134°E, and 138°E forms several mesoscale eddies (Chu et al., 2001a; 2001b). The SPF meandering near Okin Gunto (134°E) in spring was previously reported by Isoda and Saitoh (1993).

With limited data, Miyazaki (1953) found a low salinity layer in the SPF region. Later on Kim and Chung (1984) found very similar property in UTB and called it the JES Intermediate Water (JIW). After analyzing the comprehensive hydrographic data for the whole JES collected by the Japan Meteorological Agency, the Maizuru Marine Observatory, and the Hydrographic Department of the Japan Maritime Safety Agency, Senjyu (1999) showed the existence of a salinity minimum (SMIN) layer (i.e., JIW) between the TWC Water and the JES Proper Water. The southwestern JES west of 132°E is the upstream region of JIW. The lowest salinity and the highest oxygen concentration are found in the 38°– 40°N areas west of 132°E. The JIW takes two flow paths: an eastward flow along the SPF and a southward flow parallel with the Korean coast in the region west of 132°E. Analyzing the hydrographic collected from an international program, Circulation Research of the East Asian

Marginal Seas (CREAMS), Kim and Kim (1999) found the high salinity water with high oxygen in the eastern JB (i.e., north of SPF) and named the water the High Salinity Intermediate Water (HSIW).

Recently, Chu et al. (1998; 1999a) reported the seasonal occurrence of JES eddies from the composite analysis of the U.S. National Center for Environmental Prediction (NCEP)'s monthly SST fields (1981–1994). For example, they identified a warm center appearing in late spring in the East Korean Bay. Chu et al. (2001a; 2001b; 2002) further reported the seasonal variation of the thermohaline structure and inverted circulation from the Navy's unclassified Generalized Digital Environmental Model (GDEM) temperature and salinity data on a $0.5° \times 0.5°$ grid using the P-vector method (Chu, 1995). The GDEM for the JES was built on 136,509 temperature and 52,572 salinity (1930–1997) historical profiles. A three-dimensional estimate of the absolute geostrophic velocity field was obtained from the GDEM temperature and salinity fields using the P-vector method. The climatological mean and seasonal variabilities of the thermohaline structure and the inverted currents such as the SPF, the mid-level (50 to 200 m) salty tongue, the Tsushima Warm Current (TWC) and its bifurcation were identified. Using the data collected from Conductivity-Temperature-Depth (CTD) and Acoustic Doppler Current Profilers (ADCP) measurements in the southwestern JES from March to June 1992, Shin et al. (1995; 1996) found a dipole structure of gyres with an anticyclonic eddy near the Korean coast and a cyclonic eddy in the UTB.

Numerical studies of the JES circulation started in the early 1980s. Various types of models were used such as the multilayered model (Sekine, 1991; Kawabe, 1982a; 1982b; Yoon, 1982a; 1982b; Seung and Nam, 1992; Seung and Kim, 1995), the Modular Ocean Model (MOM) (Kim and Yoon, 1994; Holloway et al., 1995; Kim and Yoon, 1999; Yoshikawa et al., 1999), rigid-lid z-level model (Yoshikawa et al., 1999), the Miami Isopycnal Coordinate Model (MICOM) (Seung and Kim, 1993; Kim and Yoon, 1996) and the Princeton Ocean Model (POM) (Mooers and Kang, 1995; Chu et al., 1999b; 2000). Most of the numerical efforts are concentrated on simulating the basin-wide circulation, the TWC bifurcation, and formation of the intermediate waters using idealized or restoring-type surface thermal forcing. To date, most modelers (except Kim and Yoon, (1999)) used the restoring-type surface thermal forcing.

Kim and Yoon (1999) simulated seasonal variations of JES circulation and thermohaline structure using MOM with rigid-lid, 19 z-levels, and $(1/6)° \times (1/6)°$ horizontal resolution. The model was forced by the monthly mean wind stress (Na et al., 1992), reconstructed Haney-type surface heat flux (Haney, 1971) using climatological data (Hirose et al., 1996), and Newtonian type salinity restoring condition using observed monthly mean surface salinity. The model successfully simulates seasonal variation of the surface circulation pattern (Fig. 2), the meandering and eddy formation, and the thermohaline structure, especially the salinity minimum layer under the East Korean Warm Water (EKWC). However, the model is not able to simulate the dual gyres with an anticyclonic eddy near the Korean coast and a cyclonic eddy in UTB as observed by Shin et al. (1995; 1996). Two approaches might be useful for simulating such a dipole structure near the Korean coast: (a) implementation of a model to a realistic bottom topography, and (b) increase of the horizontal resolution. Besides, the effect of surface salinity flux (evaporation minus precipitation) on the haline structure especially the salinity minimum layer should also be studied. Hogan and Hurlbert (1999a; 1999b; 2000a; 2000b) implemented the Naval Research Laboratory Layered Ocean Model (NLOM) to JES with various horizontal resolution (up to $1/64°$) under different wind forcing. Their results demonstrate that at least $1/32°$ (3.5 km) grid is necessary to generate sufficient baroclinic instability to produce eddy-driven cyclonic deep mean flows and to obtain a realistic separation latitude of the EKWC from the Korean coast when Hellerman-Rosenstein monthly climatological wind stress forcing is used.

In this study, POM with realistic topography and flux-type surface forcing is used to simulate the seasonal variabilities of the JES circulation, and thermohaline structure including the dual gyres with an anticyclonic eddy near the Korean coast and a cyclonic eddy in UTB, the meandering SPF and eddies, the TWC bifurcation, the retroflection and dipole gyres of EKWC, the Liman Cold Current

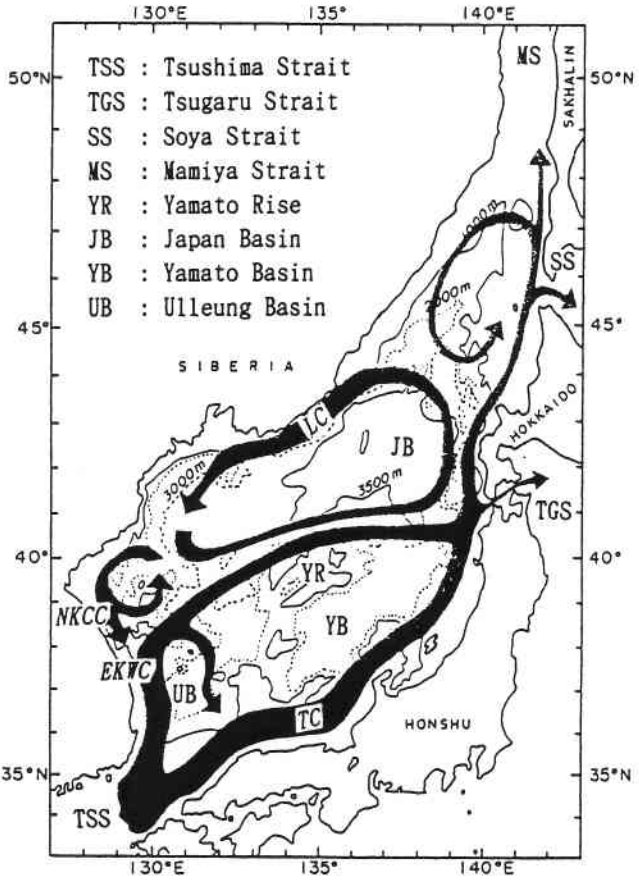

Figure 2. Schematic map of surface current systems (after Senjyu, 1999).

(LCC) and its penetration into the southwestern waters along the Korean coast, deep convection and salinity minimum layers near the SPF. These features were identified in the first part of this chapter using the Navy's GDEM data.

The outline of this chapter is as follows: A description of the JES current systems is given in Section 2. A depiction of the seasonal variation of atmospheric forcing is given in Section 3. The numerical ocean model and integration are depicted in Section 4. The simulated seasonal variability of temperature, salinity, and circulation are discussed in Sections 5, 6, and 7, respectively. In Section 8 conclusions are presented.

2. JES CURRENT SYSTEMS

Most of the nearly homogeneous water in the deep part of the basin is called the Japan Sea Proper Water (Moriyasu, 1972) and is of low temperature and low salinity. Above the Proper Water, the TWC, dominating the surface layer, flows in from the East China Sea through the Korea/Tsushima Strait and carries warm water from the south. The LCC carries cool fresh surface water from the north

and northeast (Seung and Kim, 1989; Holloway et al., 1995). The properties of this surface water are generally believed to be determined by the strong wintertime cooling coupled with freshwater input from the Amur River and the melting sea ice in Tatar Strait (Martin and Kawase, 1998). The LCC flows southward along the Russian coast, beginning at latitude slightly north of Soya Strait, terminating off Vladivostok (Fig. 2), and becoming the North Korean Cold Current (NKCC) after reaching the North Korean coast (Yoon, 1982a).

The TWC separates into two branches, which flow through the western and eastern channels of the Korea/Tsushima Strait (Kawabe, 1982a; 1982b; Hase et al., 1999). The flow through the eastern channel closely follows the Japanese Coast and is called the Nearshore Branch (Yoon, 1982c) or the first branch of TWC (FBTWC) (Hase et al., 1999). The flow through the western channel is called the EKWC, which closely follows the Korean coast until it separates near 37°N into two sub-branches. The western sub-branch moves northward and forms a cyclonic eddy over UTB off the eastern Korean coast. The eastern sub-branch flows eastward to the western coast of Hokkaido Island, and becomes the second branch of the TWC (SBTWC).

The NKCC meets the EKWC at about 38°N with some seasonal meridional migration. After separation from the coast, the NKCC and the EKWC converge and form a strong front that stretches in the zonal direction across the basin. The NKCC makes a cyclonic recirculation gyre in the north but most of the EKWC flows out through the Tsugaru and Soya Straits (Uda, 1934). The formation of NKCC and separation of EKWC are due to local forcing by wind and buoyancy flux (Seung, 1992). Large meanders develop along the front and are associated with warm and cool eddies.

Recent observation by Shin et al. (1995) shows the existence of an anticyclonic warm eddy during March to June near the Korean coast around 38°N. The length scale was approximately 150 km in surface and deepens down to about 200 m that are similar depth of the EKWC.

The surface current of the eddy reaches up to 65 cm/s while the maximum speed of the observed EKWC in June was reported as approximately 70 cm/s.

Seung (1992) identified major features of the volume transport from earlier numerical modeling results. The transport pattern is largely determined by the upper layer circulation and characterized by a large-scale cyclonic recirculation gyre, in which the EKWC and the Nearshore Branch take part as the inflow-outflow system, and also includes the NKCC. A few hundred kilometers from the separation point, the EKWC forms an anticyclonic gyre. The gyre becomes stronger as the EKWC develops. On the other hand, the northern cyclonic gyre is very deep and is most significant in winter when strengthened by the wind and buoyancy flux. It is usually called the JB gyre. The gyre, or the southward coastal current (NKCC) related to it, is deep enough to intrude southward beneath the EKWC most of the time. Seung (1992) also confirmed the summertime presence of a countercurrent beneath the Nearshore Branch.

3. SEASONAL VARIATION OF ATMOSPHERIC FORCING

3.1. General Description

The Asian monsoon strongly affects the thermal structure of the JES. During the winter monsoon season, a very cold northwest wind blows over the JES (Fig. 3a) as a result of the Siberian High Pressure System with a mean surface wind speed between 10 and 15 ms^{-1}. By late April, numerous frontally generated events occur making late April and May highly variable in terms of wind speeds and amount of clouds. During this period storms originating in Mongolia may cause strong, warm westerlies (Fig. 3b). By late May and early June, a summer surface atmospheric low pressure system begins to form over Asia. Initially this low pressure system is centered north of the Yellow Sea producing westerly winds. In late June, this low begins to migrate to the west setting up the southwest monsoon that dominates the summer months. The winds remain variable through June until the

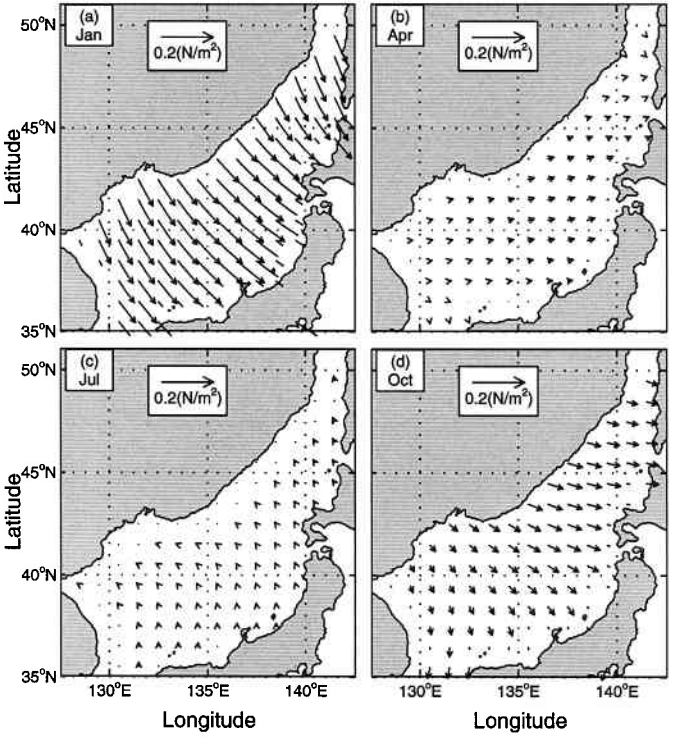

Figure 3. Climatological monthly mean wind stress for: (a) January, (b) April, (c) July, and (d) October, using the COADS data.

Manchurian Low Pressure System strengthens. Despite the very active weather systems, the mean surface wind speed over the JES in summer (Fig. 3c) is between 3 and 4 m/s, much weaker than in winter (Fig. 3a). By July, however, high pressure (the Bonin High) to the south and the low pressure over Manchuria produce southerly winds carrying warm, moist air over the East China Sea/Yellow Sea. In summer, warm air and strong downward net radiation stabilize the upper layer of the JES and causes the surface mixed layer to shoal. October (Fig. 3d) is the beginning of the transition to winter conditions. The southerly winds weaken and the sea surface slope establishes its winter pattern.

Here, a climatological description of the surface net heat and freshwater fluxes over the JES is presented. The data sets used were the objectively analyzed fields of surface marine climatology and anomalies of fluxes of heat, momentum, and freshwater. The fields are derived from individual observations in the Comprehensive Ocean-Atmosphere Data Set (COADS) from 1945 to December 1989 and are analyzed on a 1° by 1° grid (da Silva et al., 1994).

3.2. Net Surface Heat Flux

Net surface heat flux is computed by

$$Q_{Net} = R_S - (R_L + Q_S + Q_L) \tag{1}$$

where R_S is the net downward shortwave radiation, R_L the net upward longwave radiation, Q_S the sensible heat flux, and Q_L the latent heat flux. Positive (negative) values of Q_{Net} indicate net heat

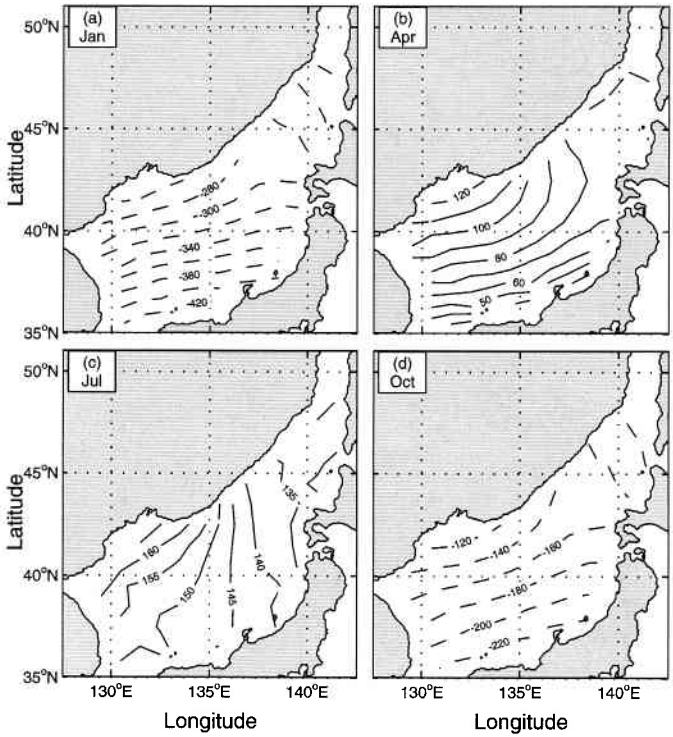

Figure 4. Climatological monthly mean net heat flux (W m^{-2}) for: (a) January, (b) April, (c) July, and (d) October, using the COADS data.

gain (loss) of the ocean at the surface. The summer field is relatively homogeneous (140 to 160 W m^{-2}) throughout the JES, whereas a significant horizontal gradient increasing from the southeast (Japan coast) to the northwest (Russian coast) exists for the other seasons (Fig. 4). The ocean surface near Korea/Tsushima Strait has a maximum heat loss of 400 W m^{-2} in the winter (January) and a minimum heat gain of 60 W m^{-2} in the spring (April). This range of values is consistent with earlier studies (Hirose et al., 1996; Seo, 1998). This long-term net surface heat loss will be compensated by the advection of warm waters from the East China Sea.

3.3. Surface Freshwater Flux

The surface freshwater flux is the difference between precipitation rate (P) and evaporation rate (E)

$$F = P - E \tag{2}$$

Positive values of F indicate net water mass gain at the sea surface. The surface freshwater flux exhibits a distinct four-season pattern. The winter is characterized by freshwater gain (2 to 6 cm/month) in the northern and northeastern JES, and freshwater loss (2 to 10 cm/month) in the southern and southwestern JES. A strong horizontal F-gradient monotonically decreases from northeast to southwest. The spring (Fig. 5b) and summer (Fig. 5c) are both characterized by freshwater gain in the whole JES with different horizontal F-gradients: decreasing (increasing) from 4 cm/month

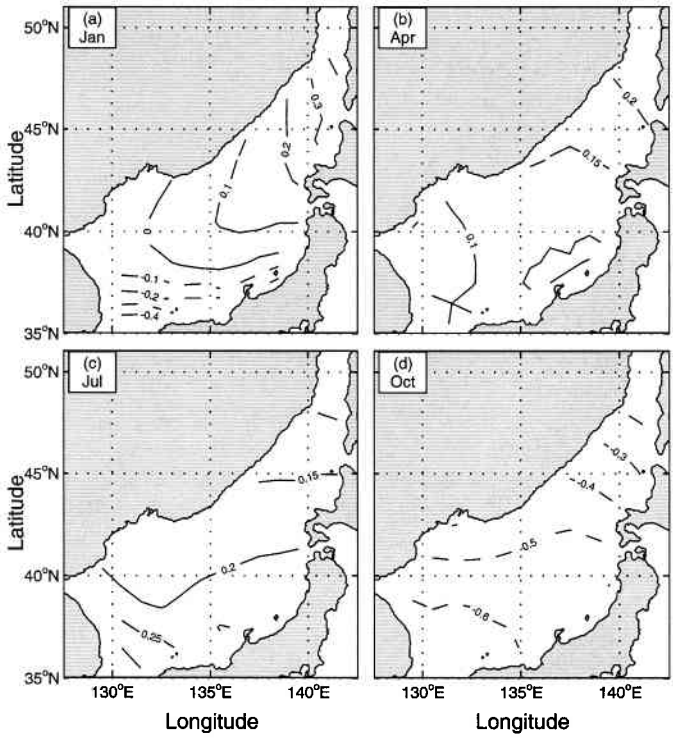

Figure 5. Climatological monthly mean precipitation minus evaporation [mm (3 hr)$^{-1}$] for: (a) January, (b) April, (c) July, and (d) October, using the COADS data.

(4 cm/month) in the northeast JES to 2 cm/month (6 cm/month) in the southwest JES in the spring (summer). The autumn (Fig. 5d) is characterized by freshwater loss in the whole JES (4 to 16 cm/month) with a maximum loss of 16 cm/month near Korea/Tsushima Strait.

4. NUMERICAL OCEAN MODEL

4.1. Model Description

Coastal oceans and semi-enclosed seas are marked by extremely high spatial and temporal variability that challenges the existing predictive capabilities of numerical simulations. POM is a time-dependent, primitive equation circulation model rendered on a three-dimensional grid that includes realistic topography and a free surface (Blumberg and Mellor, 1987). Tidal forcing was not included in this application of the model, since high frequency variability of the circulation is not considered. River outflow is also not included. However, the seasonal variation in sea surface height, temperature, salinity, circulation, and transport are represented by the model. From a series of numerical experiments, the qualitative and quantitative effects of nonlinearity, wind forcing, and lateral boundary transport on the JES is analyzed, yielding considerable insight into the external factors affecting the regional oceanography.

Consequently, the model contains 181 × 199 × 23 fixed grid points. The horizontal spacing is 5′ latitude and longitude (approximately 5.77 to 7.59 km in the zonal direction and 9.265 km in

the meridional direction) and there are 23 sigma levels in vertical coordinate. The model domain extends from 35.0°N to 51.0°N, and from 127.0°E to 142.0°E. The bottom topography (Fig. 1) is obtained from the Naval Oceanographic Office's Digital Bathymetry Data Base 5′× 5′ resolution (DBDB5). The horizontal friction and mixing are modeled using the Smagorinsky (1963) form with the coefficient chosen to be 0.2 for this application. The bottom stress τ_b is assumed to follow a quadratic law

$$\boldsymbol{\tau}_{\mathbf{b}} = \rho_0 |\mathbf{V_b}| \mathbf{V_b} \tag{3}$$

where ρ_0 (= 1025 kg/m^3) is the characteristic density of the sea water, $\mathbf{V_b}$ is the horizontal component of the bottom velocity, and C_D is the drag coefficient which is specified as 0.0025 (Blumberg and Mellor, 1987), which is similar to the value (0.002) used by Hogan and Hurlburt (2000a).

4.2. Surface Forcing Functions

The atmospheric forcing for the JES application of POM includes mechanical and thermohaline forcing. The wind forcing is depicted by

$$\rho_0 K_M \left(\frac{\partial u}{\partial z}, \frac{\partial v}{\partial z} \right)_{z=0} = (\tau_{0x}, \tau_{0y}) \tag{4}$$

where K_M is the vertical mixing coefficient for momentum, (u, v) and (τ_{0x}, τ_{0y}) are the two components of the water velocity and wind stress vectors, respectively. The wind stress at each time step is interpolated from monthly mean climatological wind stress from COADS (1945–1989), with a resolution of 1° × 1°. The COADS wind stress was interpolated into the model grid with a resolution of 5′.

Surface thermal forcing is depicted by

$$K_H \frac{\partial \theta}{\partial z} = \alpha_1 \left(\frac{Q_H}{\rho C_p} \right) + \alpha_2 C \left(\theta_{OBS} - \theta \right) \tag{5}$$

$$K_S = \frac{\partial S}{\partial z} = -\alpha_1 FS + \alpha_2 C \left(S_{OBS} - S \right) \tag{6}$$

where K_H and K_S are the vertical mixing coefficients for heat and salt, (θ, S) and (θ_{OBS}, S_{OBS}) are modeled and observed potential temperature and salinity, and c_p is the specific heat. The relaxation coefficient C is the reciprocal of the restoring time period for a unit volume of water. The parameters (α_1, α_2) are (0, 1) switches: α_1 = 1, α_2= 0, would specify only flux forcing is applied. The flux forcing is used in this study.

4.3. Lateral Boundary Forcing

Boundary conditions for closed lateral boundaries, (i.e., the modeled ocean) bordered by land, were defined using a free-slip condition for velocity and a zero gradient condition for temperature and salinity. Thus, no advective or diffusive heat, salt or velocity fluxes occur through these boundaries.

At open boundaries, the numerical grid terminates but the fluid motion is unrestricted. Uncertainty at open boundaries makes marginal sea modeling difficult. Three approaches, local-type, inverse-type, and nested-basin/coastal modeling, are available for determining the open boundary condition. Here, we take the local-type approach; i.e., use the radiation boundary condition with specified volume transport. When the water flows into the model domain, temperature and salinity at the open boundary are prescribed from observational data. When water flows out of the domain, the radiation condition was applied

$$\frac{\partial}{\partial t} (\theta, S) + U_n \frac{\partial}{\partial n} (\theta, S) = 0 \tag{7}$$

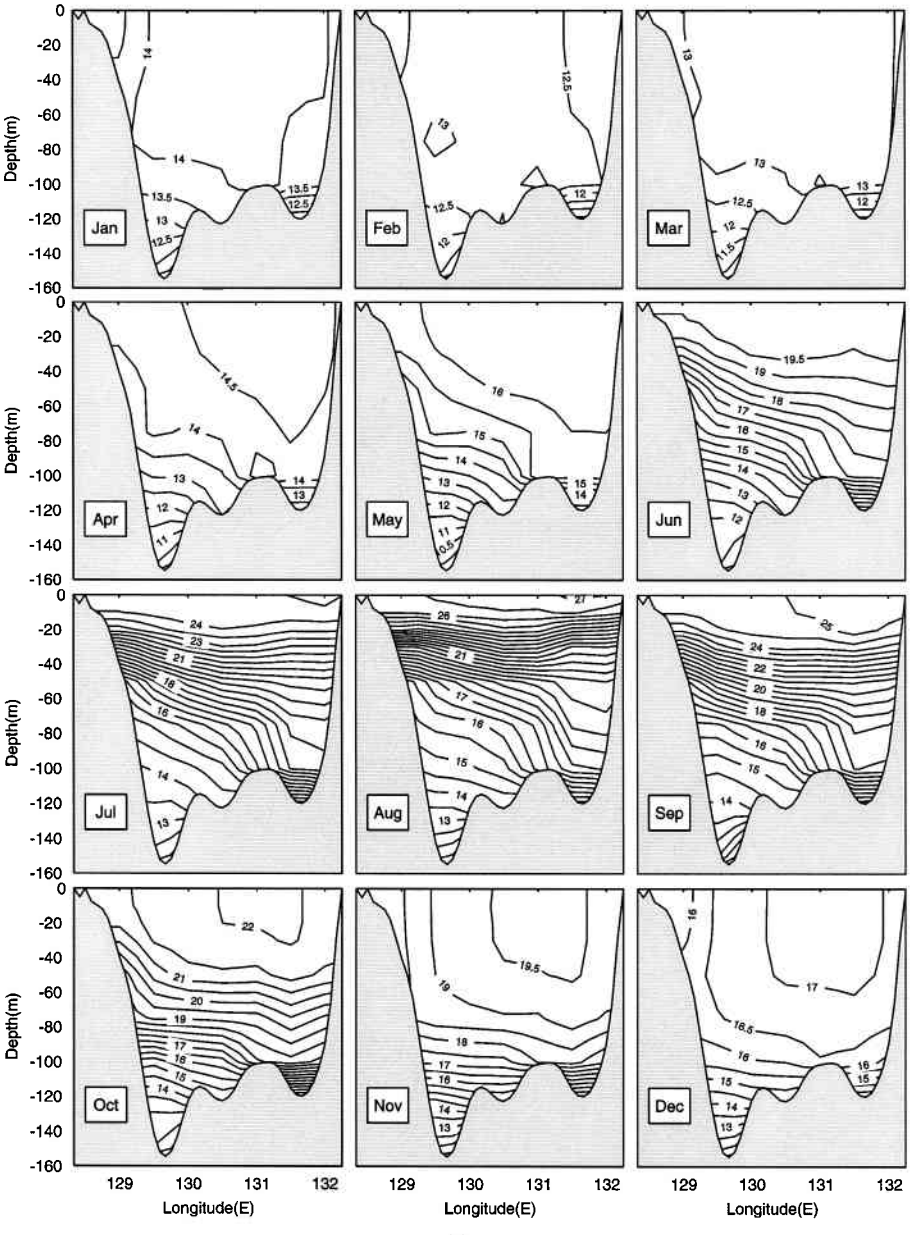

(a)

Figure 6. (a) Vertical cross-sections of monthly mean temperature (°C) at the Tsushima/Korea Strait.

where the subscript n denotes the direction normal to the boundary.

The temperature and salinity values at the open boundaries can be either obtained from historical data such as the Navy's Master Oceanographic Observational Data Set (MOODS), or monthly mean climatological data such as the Navy's Generalized Digital Environmental Model (GDEM) data (Chu

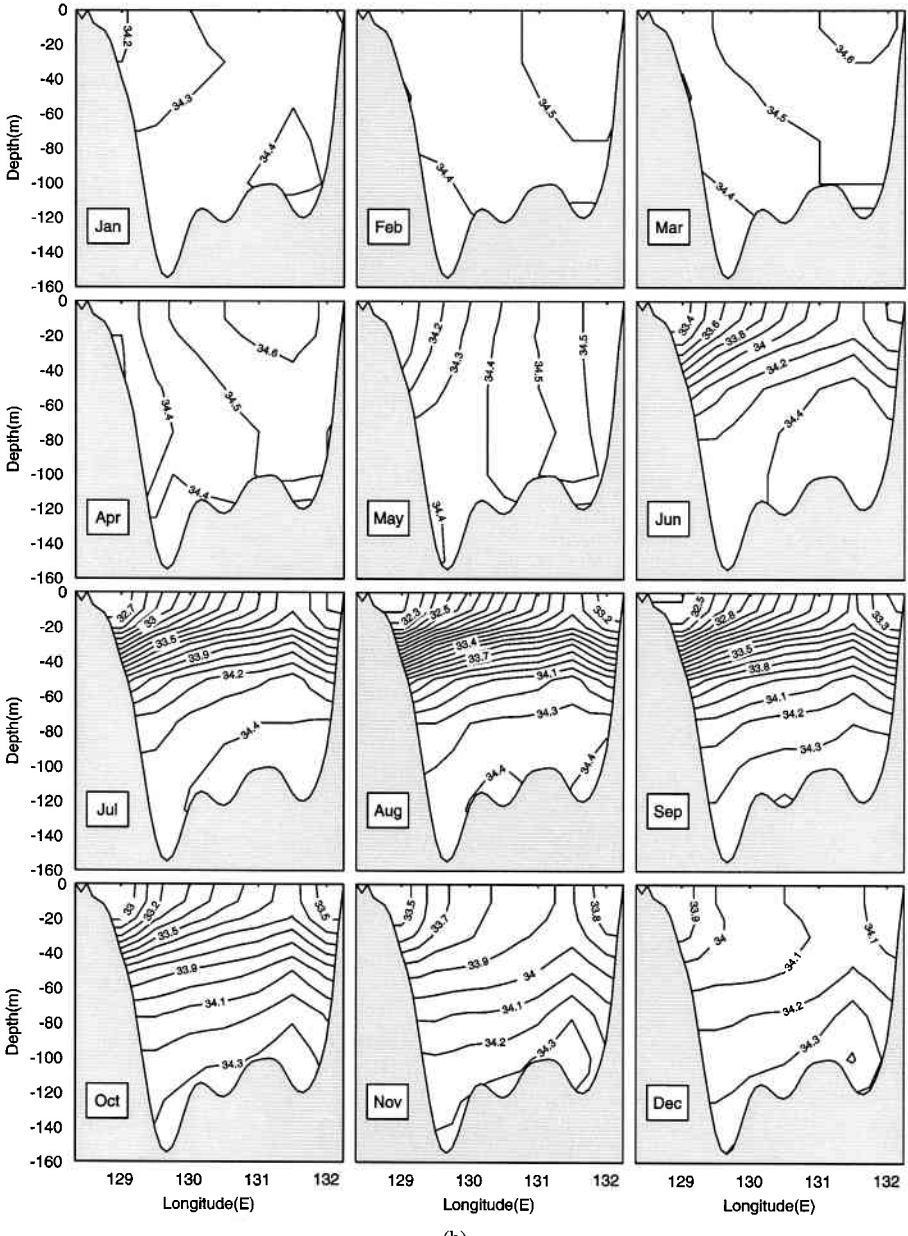

(b)

Figure 6. (b) Vertical cross-sections of monthly mean salinity (ppt) at the Tsushima/Korea Strait.

et al., 2000). For simulating the seasonal variability, we use the GDEM T, S data at the open boundaries. Vertical cross-sections of monthly mean temperature (Fig. 6a) and salinity (Fig. 6b) at the Korea/Tsushima Strait show the seasonal variability of a warm-core and a salt-core. The warm-core occupies a large portion of the Korea/Tsushima Strait during the winter monsoon season (Novem-

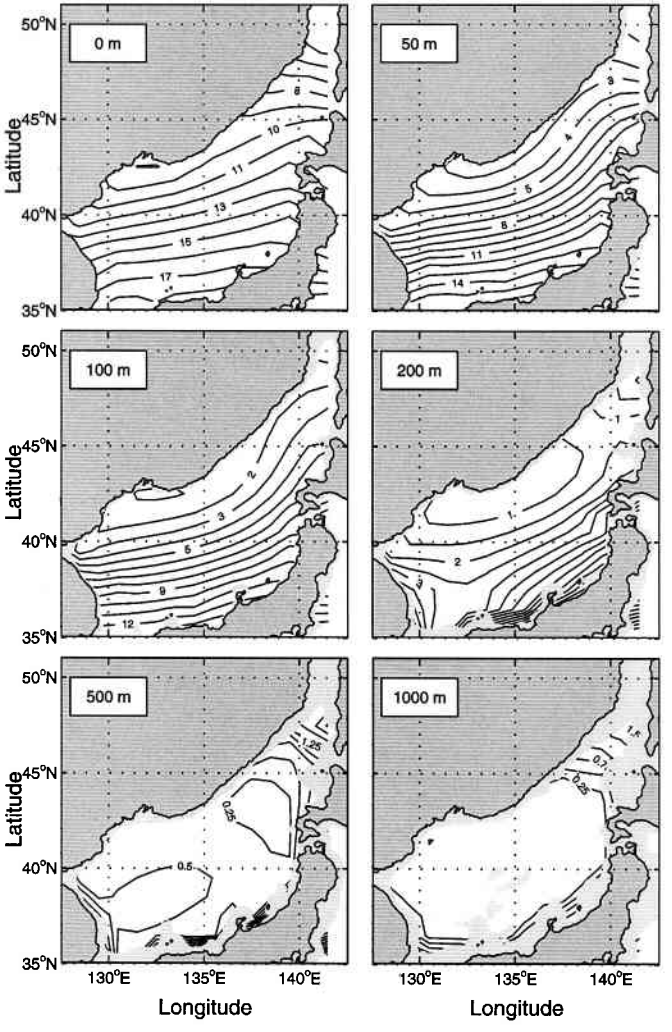

(a)

Figure 7. (a) Initial fields from the climatological data (Levitus, 1982) at different depths: temperature (°C).

ber to March) and weakens and shoals during the summer monsoon season (June to August). In the summer, the water at the Korea/Tsushima Strait is strongly stratified (Figs. 7a and 7b).

The volume transports at open boundaries are specified from historical data. Positive (negative) values are referred to inflow (outflow). Warm water enters the JES through the Korea/Tsushima Strait with the TWC from the East China Sea and exits the JES through the Tsugaru and Soya straits. There is no evident volume transport through the Tatar Strait (Martin and Kawase, 1998), which was taken as zero in this study. Recent estimates of the monthly mean volume transport, reported by Yi (1966), through the Korea/Tsushima Strait with the annual average of 1.3 Sv, a maximum of 2.2 Sv in October, and a minimum of 0.3 Sv in February. Bang et al. (1996) used the maximum inflow transport of about 3.5 Sv in August and minimum of 1.6 Sv in February, while Kim and Yoon (1999) used the mean value of 2.2 Sv with $\pm$ 0.35 Sv with the maximum in mid-September and the

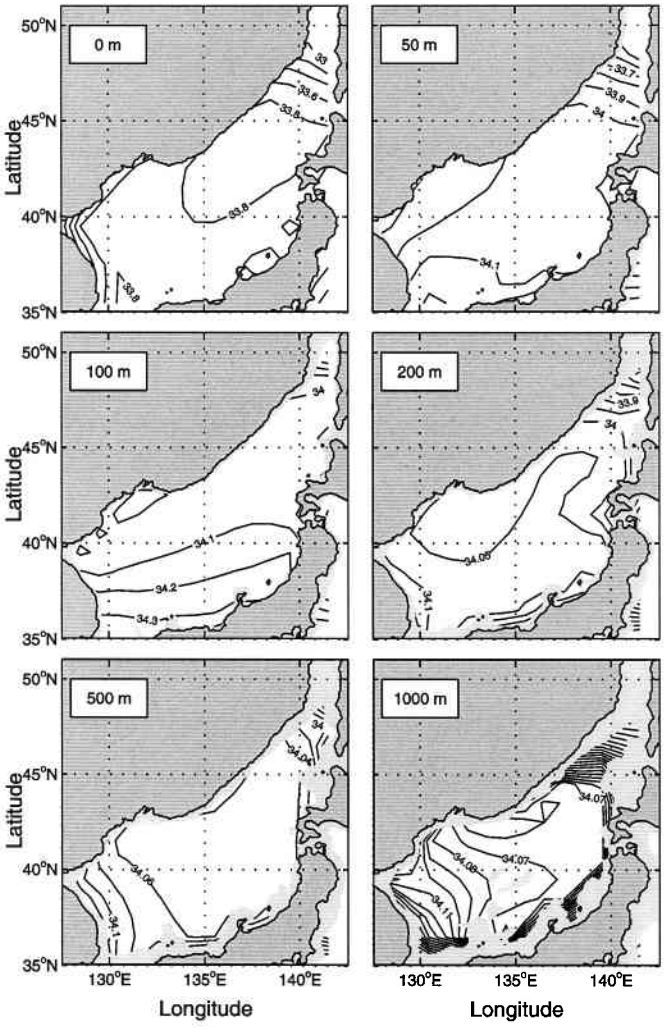

(b)

Figure 7. (b) Initial fields from the climatological data (Levitus, 1982) at different depths: salinity (ppt).

minimum in mid-March. The total inflow transport through Korea/Tsushima Straits should be the same as the total outflow transport through the Tsugaru and Soya Straits. We assume that 75% (80% in Bang et al., 1996) of the total inflow transport should flow out of the JES through the Tsugaru Strait, and 25% (20% in Bang et al., 1996) through the Soya Strait. This ratio is adopted from the maximum volume transport through the Tsugaru Strait estimated by Toba et al. (1982), and through the Soya Strait estimated by Preller and Hogan (1998). The monthly volume transports through open boundaries are listed in Table 1.

4.4. Mode Splitting

For computational efficiency, the mode splitting technique (Blumberg and Mellor, 1987) is applied with a barotropic time step of 25 seconds, based on the Courant-Friederichs-Levy computational

Table 1
Monthly values of volume transport (Sv) through the lateral open boundaries. The positive/negative values mean inflow/outflow.

Month	Jan	Feb	Mar	Apr	May	Jun	Jul	Aug	Sep	Oct	Nov	Dec
Soya	-0.2	- 0.08	- 0.08	- 0.13	- 0.23	- 0.33	- 0.43	- 0.53	- 0.55	- 0.53	- 0.48	- 0.35
Tatar	0.0	0.0	0.0	0.0	0.0	0.0	0.0	0.0	0.0	0.0	0.0	0.0
Tsugaru	- 0.6	- 0.22	- 0.22	- 0.37	- 0.67	- 0.97	- 1.27	- 1.57	- 1.65	- 1.57	- 1.42	- 1.05
Tsushima	0.8	0.3	0.3	0.5	0.9	1.3	1.7	2.1	2.2	2.1	1.9	1.4

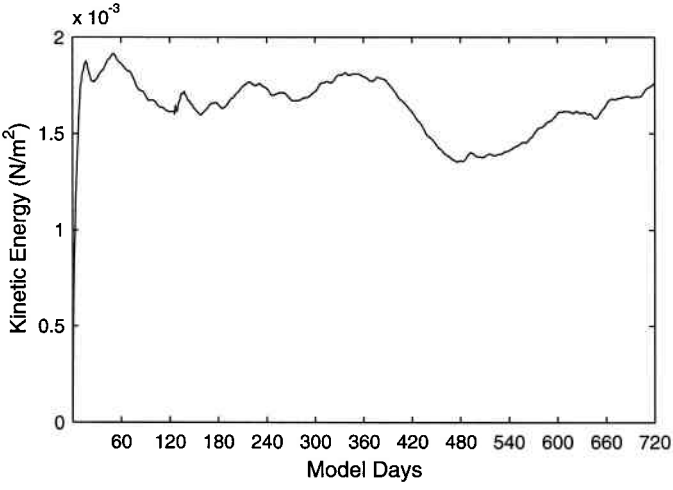

Figure 8. Temporal variation of kinetic energy per unit volume (N m^{-2}) during the model initialization.

stability (CFL) condition and the external wave speed; and a baroclinic time step of 900 seconds, based on the CFL condition and the internal wave speed.

4.5. Two-Step Initialization

Two steps are used to initialize POM. During the first step (restoring run), POM is integrated for two years from zero velocity and climatological temperature (Fig. 7a) and salinity (Fig. 7b) fields (Levitus, 1982) with climatological monthly mean surface wind stress from the COADS data and restoring-type surface thermohaline forcing ($\alpha_1 = 0$, $\alpha_2 = 1$) which are relaxed to surface monthly mean values. The climatological monthly mean field (Fig. 7a) shows that the horizontal temperature gradient is quite uniform in the JES basin (i.e., SPF is not evident).

It was found that 90 days were sufficient for the model kinetic energy to reach quasi-steady state under the imposed conditions (Fig. 8). The final states of the restoring run are taken as initial conditions for the second step (simulation run). During the simulation run, POM is integrated again for two more years with climatological monthly mean surface wind stress, net heat flux, and freshwater flux ($\alpha_1 = 1$, $\alpha_2 = 0$) from the COADS data. The simulated temperature and salinity fields are consistent with observational studies reported in Section 1 of this chapter.

5. TEMPERATURE

5.1. Sea Surface Temperature

The simulated monthly sea surface temperature (SST) is examined (Fig. 9). Comparing to the initial temperature field (Fig. 7a), the model simulated the formation of the Sub-Polar Front (SPF). Although SST field (Fig. 9) shows an evident seasonal variation, the SPF exists at all times throughout the year with mean latitude around 41°N. Its position is quite stationary, but its intensity strengthens in the winter and weakens in the summer. Such a pattern is similar to earlier descriptions (Maizuru Marine Observatory, 1997; Chu et al., 2001a). The location of the SPF in spring is quite consistent with Isoda and Saitoh's (1993) estimations using ten NOAA-8 satellite Advanced Very High Resolution Radiometer (AVHRR) images in spring 1984.

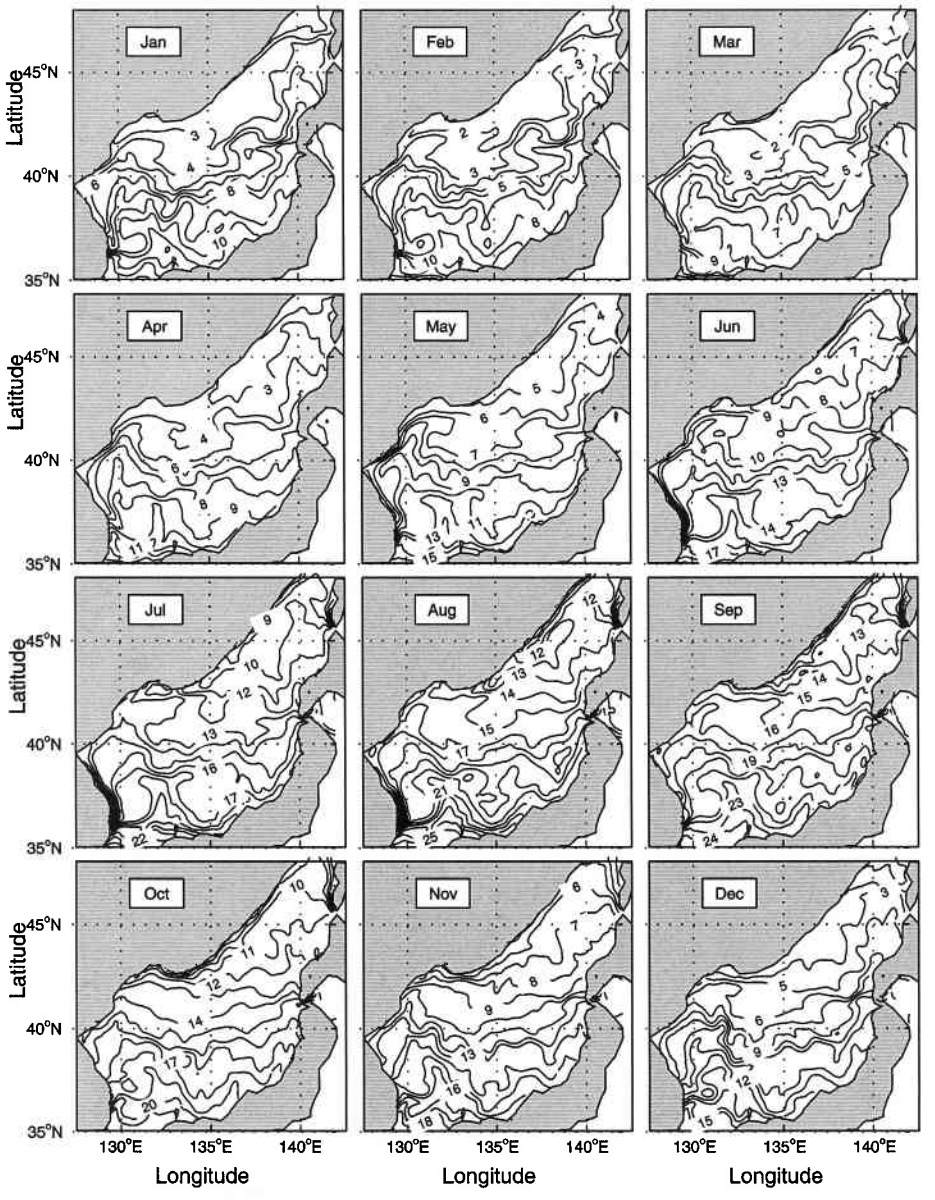

Figure 9. Simulated monthly mean sea surface temperature (°C) field.

In the simulation of Kim and Yoon (1999), the Location of the SPF was about 1° northward compared to the observed temperature field (Fig. 2 in their paper), and the water temperatures in the SPF area were 2–3°C higher than the observation. Comparison of Fig. 9 with Fig. 2 in Kim and Yoon (1999) signifies improvement of model performance in predicting the SPF location and the temperature field especially in winter.

The SST is always found higher in the UTB than in the YB, which is consistent with Kim and Kim's (1999) observational studies. The SST gradient across the SPF is twice as strong in the winter as in the summer. The weakening of the SPF in the summer is caused by the faster warming of the waters north of SPF than that of the waters south of it in the spring. North of the SPF a second front occurs (bi-frontal structure) during the fall-to-winter transition season, especially in November and December. This front parallels the Russian coast with the maximum SST gradient around 4°C/100 km in November.

5.2. Zonal Cross-Sections (37° and 43°N)

The zonal cross-sections (37° and 43°N) of the simulated monthly mean temperature show a strong seasonal/permanent thermocline structure south of the SPF (Fig. 10a) and a strong seasonal/weak permanent thermocline structure north of the SPF (Fig. 10b).

South of the SPF at 37°N (Fig. 10a), the permanent thermocline is located at 80 to 250 m and appears throughout the year with the maximum strength (0.08°C m^{-1}) in August. Above it, the seasonal thermocline occurs from the surface to 50 m depth in June (0.15°C m^{-1}), intensifies during the summer monsoon season to a maximum value of around 0.36°C m^{-1} in August, and weakens in September. In October, the seasonal thermocline erodes and the ocean mixed layer (OML) starts to occur. In November, the OML is well-established with the temperature near 14°C and the depth around 75 m. During the prevailing winter monsoon season (December to March), the OML deepens to 80–100 m with a westward uplift of the OML depth: 50 m near the Korean coast and 130 m near the Japanese coast. The OML starts to warm in March, and its depth shoals rapidly. The OML depth decreases from 50–100 m in March to less than 10 m in April. This process (OML warming and shoaling) continues during the summer monsoon season (June-August). The OML shoaling simulated using POM is a month earlier compared to the observational data (Section 1 of this chapter).

North of SPF at 43°N (Fig. 10b), the permanent thermocline is quite weak. The seasonal thermocline occurs from the surface to 50 m depth in May ($\sim$ 0.08°C m^{-1}), intensifies during the summer monsoon season to a maximum value of around 0.5°C m^{-1} in August and September, and weakens in October. In November, the seasonal thermocline erodes and becomes the part of the permanent thermocline, which weakens during the prevailing winter monsoon season. In February, the permanent thermocline is so weak that the water column is almost uniformly cold (1°C) west of 136°E, and weakly stratified ($\leqslant$ 0.01°C m^{-1}) east of 136°E.

5.3. Meridional Cross-Section (135°E)

The strong north-south thermal asymmetry across the SPF is also seen from the meridional cross-section (135°E) of the monthly mean temperature (Fig. 11). North of the SPF, the seasonal thermocline occurs near the surface in April and May, enhances in summer, and is still quite strong with a vertical gradient of 0.12°C m^{-1} in October. It weakens drastically in November. South of the SPF, the seasonal thermocline occurs in summer monsoon season, weakens in early fall, and disappears in November. The winter convection (December to March) is very evident north of the SPF ($\sim$ 41°N). This is consistent with the observational study reported by Seung and Yoon (1995).

During the prevailing winter monsoon season (December to March), the simulated permanent thermocline is identified at 100 to 300 m deep south of the SPF with a vertical temperature gradient weakening from December (near 0.05°C m^{-1}) to March (near 0.025°C m^{-1}). The simulated permanent thermocline is much weaker north of the SPF. From January to March, there is almost no evident thermocline north of the SPF.

During the prevailing summer monsoon season (June to August), a shallow seasonal thermocline occurs with a much greater strength north of the SPF than south of the SPF; and overlays relatively uniform water north of the SPF and stratified water (the permanent thermocline) south of the SPF. North of the SPF a seasonal thermocline appears near the surface (above 50 m depth) with a vertical

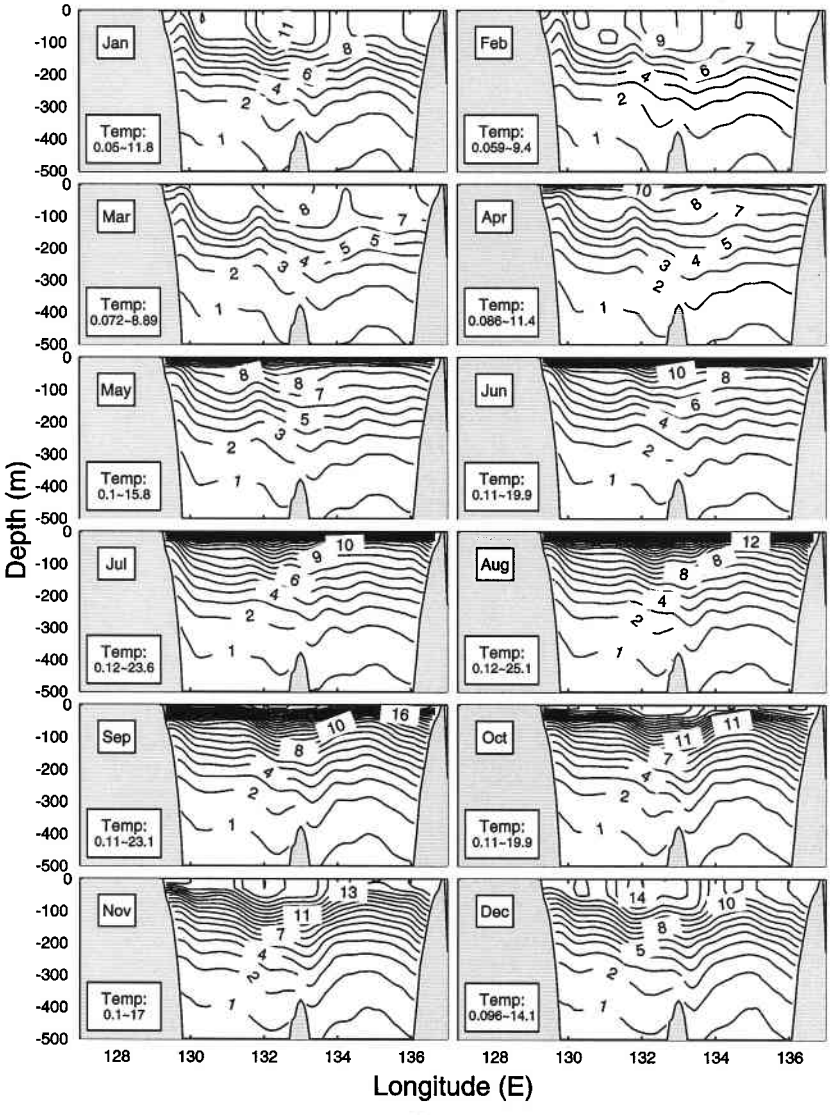

(a)

Figure 10. (a) Simulated zonal cross-section of the monthly mean temperature (°C): 37°N.

gradient enhancing from 0.25°C m^{-1} in June to 0.36°C m^{-1} in August. This strong and shallow thermocline isolates the exchange of the seawater below the thermocline from the atmospheric forcing and makes this water (north of the SPF under the thermocline) quite uniform. South of the SPF, the seasonal thermocline is wider (25 to 100 m deep) and weaker with a vertical gradient around 0.13°C m^{-1}. Such a north-south asymmetric pattern was previously presented by Kim and Kim (1999) using the Circulation Research of the East Asian Marginal Seas (CREAMS) data taken mainly in July 1995, and by Chu et al. (2000) using the GDEM data.

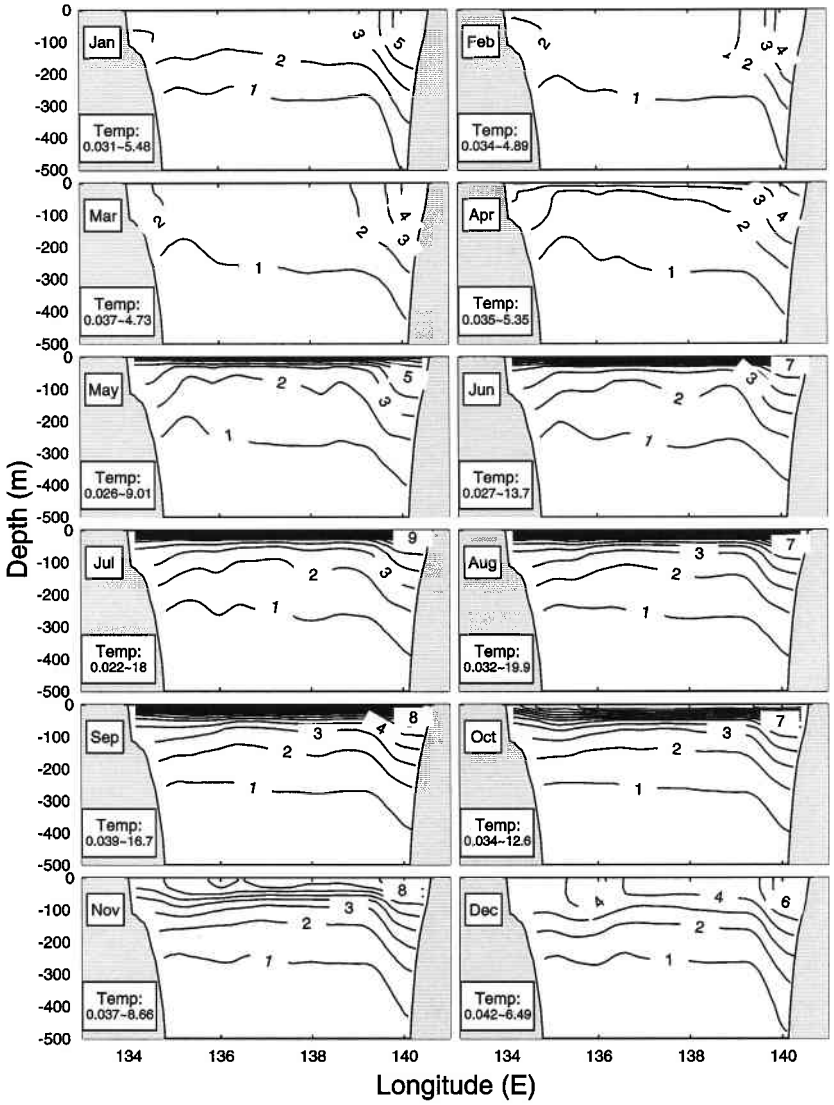

(b)

Figure 10. (b) Simulated zonal cross-section of the monthly mean temperature: 43°N.

6. SALINITY

6.1. Sea Surface

The most striking feature of the simulated monthly sea surface salinity (SSS) field (Fig. 12) is the existence of a strong salinity gradient in the far north of JES with low salinity waters along the continental coastal area. For the JES basin, the saline Kuroshio water enters the JES through the Korea/Tsushima Strait and forms two permanent salty centers located in the northern JB (west of Hokkaido Island), with the salinity higher than 34.0 ppt, and the area between UTB and YB with

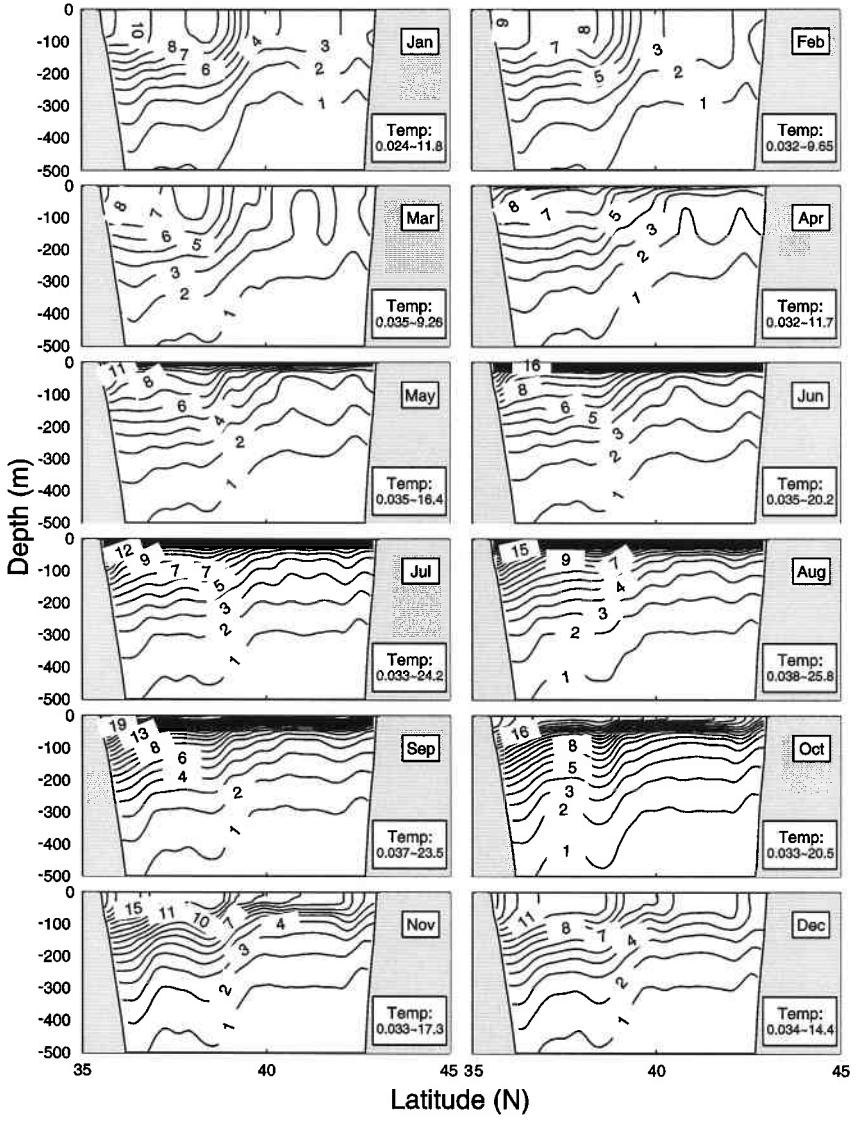

Figure 11. Simulated latitudinal cross-section (135°E) of the monthly mean temperature (°C) along 135°E.

the maximum salinity of 34.3 ppt in August-September, respectively. The northern JB salty center has less seasonal variation than the UTB/YB salty center. Around the UTB/YB salty center, there are several fresh centers occurring largely from late summer to fall-early winter. The simulated winter (February) field (Fig. 12) is consistent with that reported by Kim and Kim (1999, Fig. 9 in their paper) using the data set of the Japan Oceanographic Data Center from 1930 to 1990.

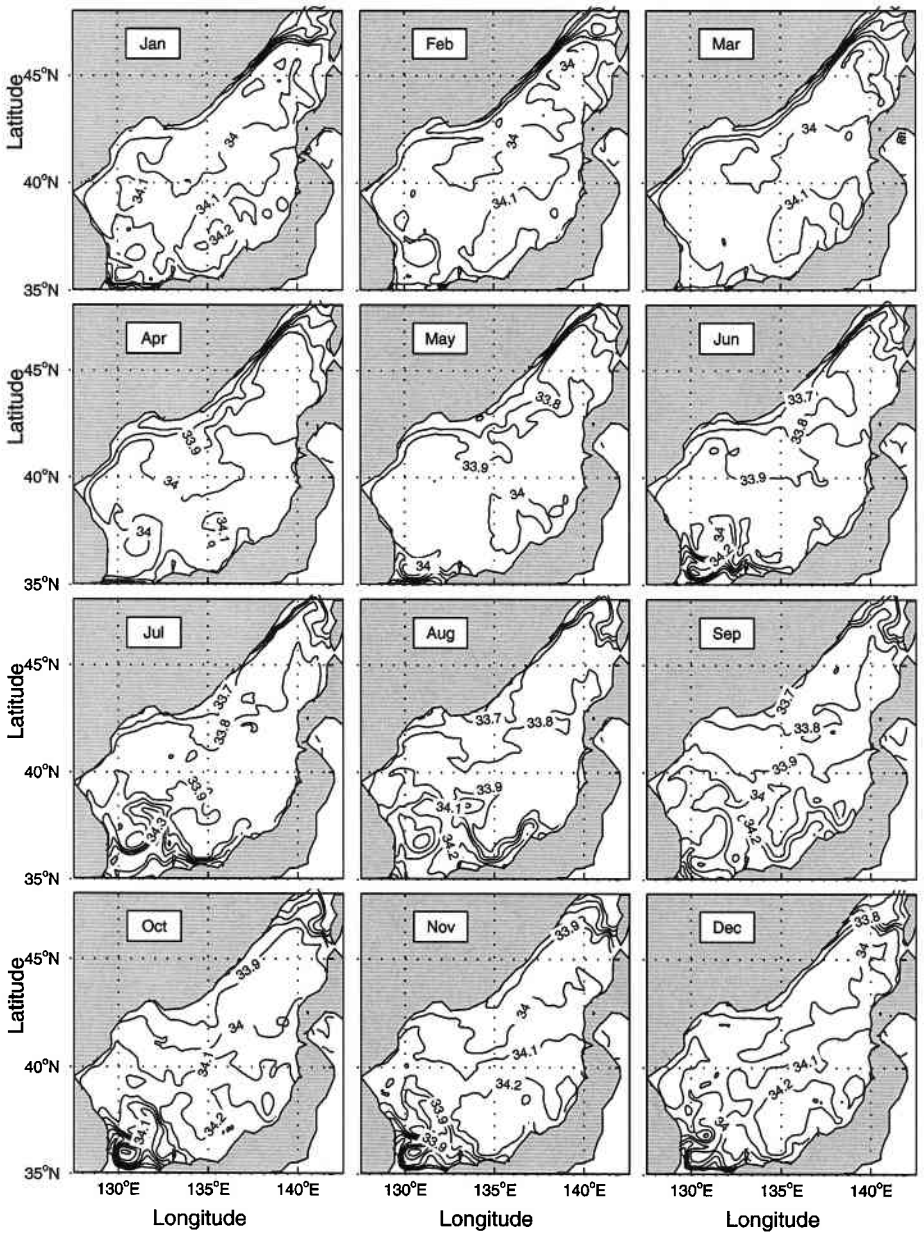

Figure 12. Simulated monthly mean sea surface salinity (ppt) field.

6.2. Zonal Cross-Sections (37° and 43°N)

The zonal cross-sections (37° and 43°N) of the simulated monthly mean salinity show an evident sublayer (200 to 300 m) SMIN south of the SPF (Fig. 13a) and absence of a SMIN north of the SPF

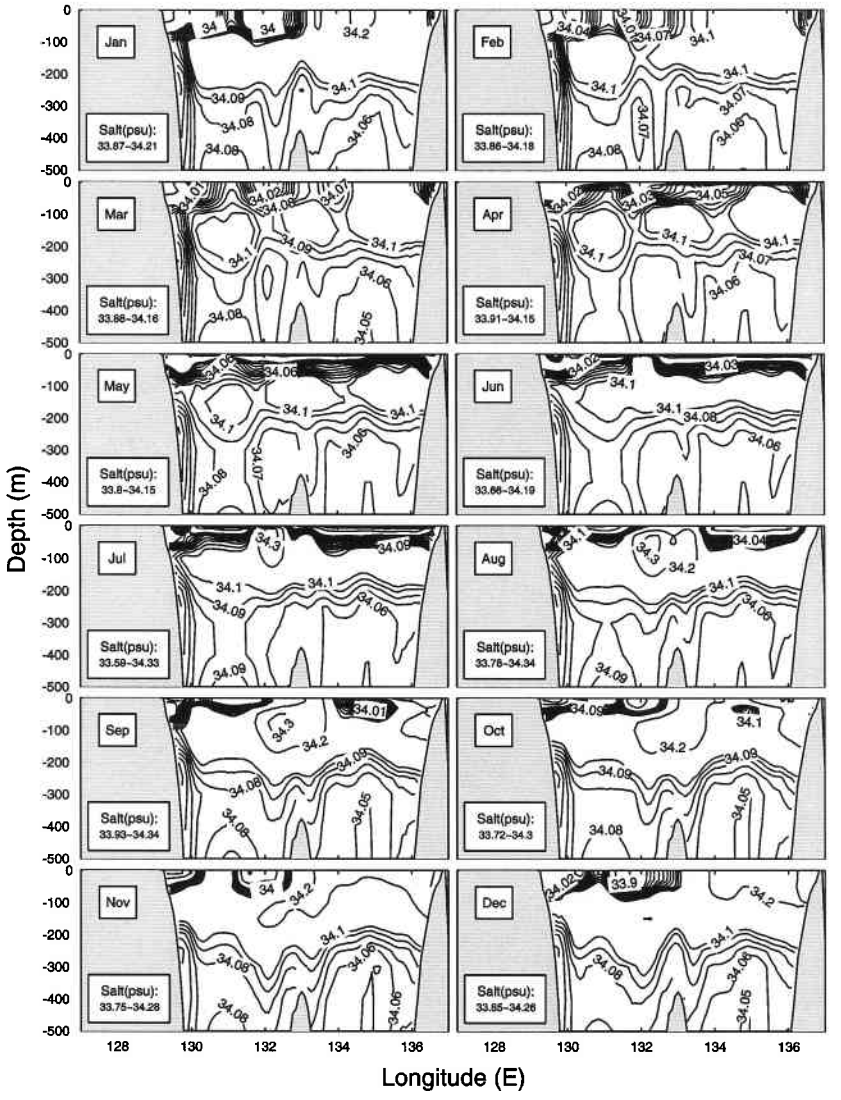

(a)

Figure 13. (a) Simulated zonal cross-section of the monthly mean salinity (ppt): 37°N.

(Fig. 13b). The water with salinity of about 34.08 ppt in the eastside of 134°E around the depth of about 200 m are located under more saline water in the surface layer that has the characteristics of the TWC. The low saline water throughout the water column in high latitude (Fig. 13b) is the typical coastal water that advects to southward under the TWC, and forms the SMIN (Kim and Kim, 1999; Kim and Yoon, 1999). This consists with many earlier studies such as Miyazaki (1952, 1953), Kim and Chung (1984), Senjyu (1999), and Chu et al. (2000).

South of the SPF at 37°N (Fig. 13a), a strong seasonal halocline occurs from the surface to 30 m depth in June (0.01 ppt m^{-1}), intensifies during the summer monsoon season to a maximum value of

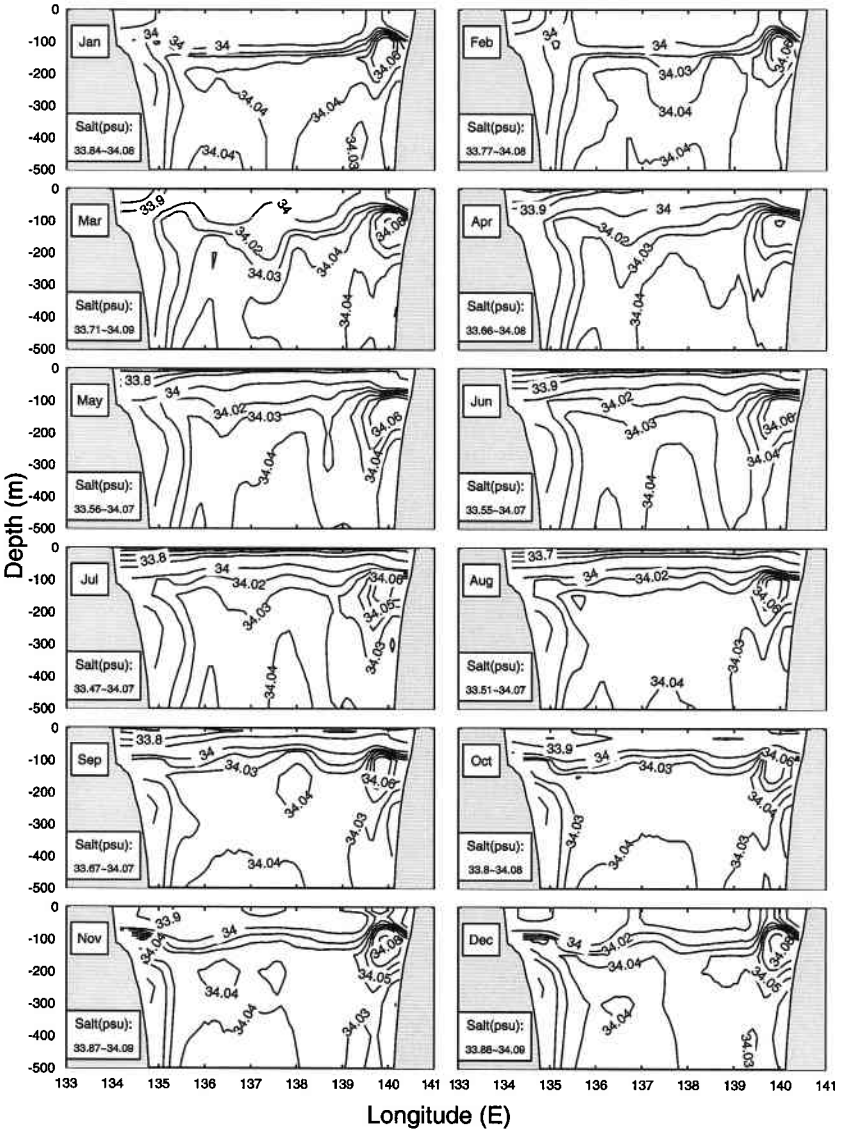

(b)

Figure 13. (b) Simulated zonal cross-section of the monthly mean salinity (ppt): 43°N.

around 0.02 ppt m^{-1} in August, and weakens from September to December. In January, the seasonal halocline erodes and disappears. A horizontally oriented salinity maximum (SMAX) ($S > 34.1$ ppt) usually broken into several salty parts appears in winter and spring above the SMIN with the interface at 200 to 300 m depths.

North of the SPF at 43°N (Fig. 13b), the SMIN shows up in the upper layer (above 100 m) of the western JB (west of 136°E) throughout the year. This is consistent with Kim and Kim's (1999)

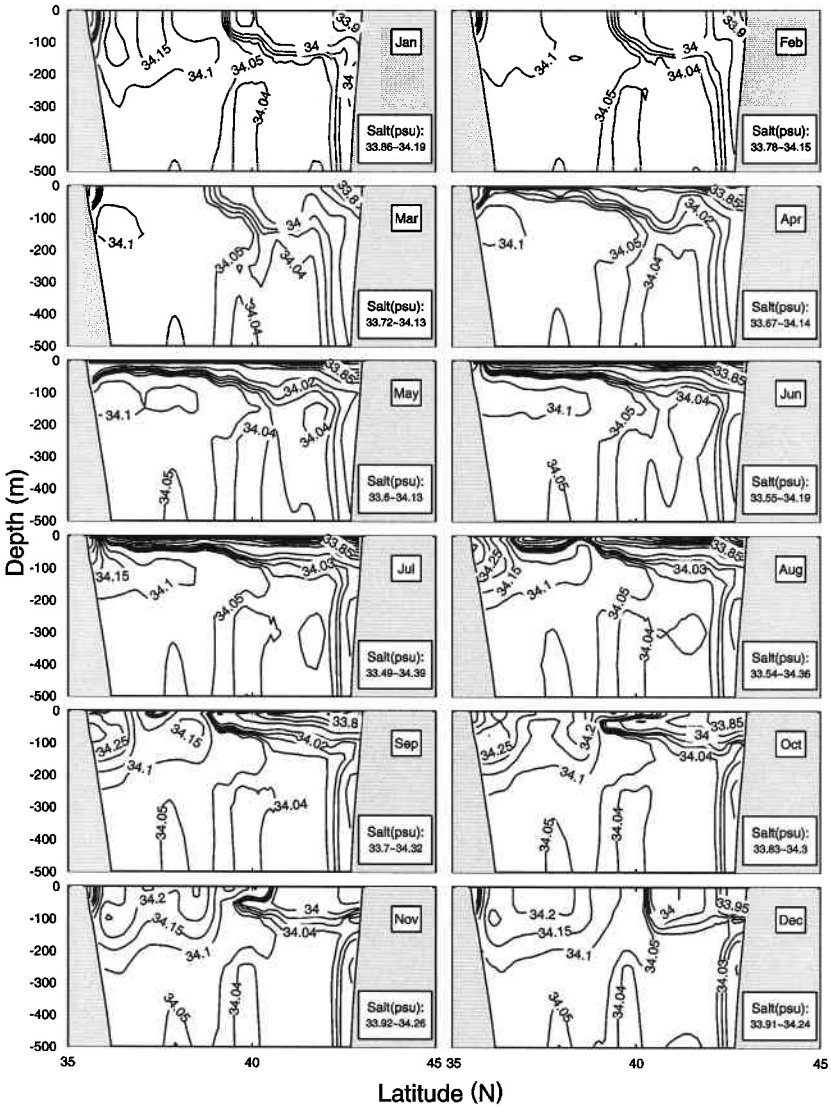

Figure 14. Simulated latitudinal cross-section (135°E) of the monthly mean salinity (ppt) along 135°E.

identification that the JIW in the western JB is characterized by a low salinity ($S < 34.00$), and the HSIW in the eastern (139°–140°E) JB is featured by high salinity ($S > 34.05$ ppt).

6.3. Meridional Cross-Section (135°E)

The strong north-south haline asymmetry across the SPF is also simulated from the meridional cross-section (135°E) of the monthly mean salinity; the appearance (disappearance) of the SMIN south (north) of the SPF (Fig. 14).

From the surface layer in high latitudes the low saline water penetrates into the intermediate depth of about 200 to 300 m during the summer monsoon season (July-October) underneath tongue-shaped saline water of the TWC. The SMAX with a salty core ($S > 34.05$ ppt) is simulated below the SMIN layer north of SPF.

The SMAX with a salty core ($S = 34.3$ ppt) was observed in October 1969 when a hydrographic survey for the whole JES basin was carried out by the Japan Meteorological Agency (Kim and Kim, 1999). The interface between the SMIN and the SMAX is located at 100 to 200 m deep. During the winter monsoon season, the SMIN is not evidently shown.

7. CIRCULATION

7.1. General Description

The simulated surface velocity field (Fig. 15) coincides with earlier description of JES circulation presented in Section 2. The TWC separates at the Korea/Tsushima Strait into two branches through a western and an eastern channel. Flow through the western channel (i.e., EKWC) closely follows the Korean coast until it separates near 38°N into two branches. The eastern branch follows the SPF to the west coast of Japan, and the western branch, flows northward and forms a cyclonic eddy in the southern UTB. The LCC carries fresh and cool water along the Russian coast and becomes the NKCC at the North Korean coast. The NKCC meets the EKWC at about 38°N. After separation from the coast, the NKCC and the EKWC converge to form a strong zonal jet across the basin.

7.2. Liman Cold Current

The LCC is a southwestward current following along the Russian coast. It bifurcates into two branches near Vladivostok: the western branch flows along the Russian-Korean coast and becomes the NKCC. The eastern branch flows southeastward, then turns eastward at 41.5°N, and becomes the southern flank of the JB gyre. The LCC has a strong seasonal variation with a maximum speed in winter and a minimum speed in the summer (Fig. 15).

Zonal cross-sections of the meridional velocity at 46°N for January (winter), April (spring), July (summer), and October (fall) indicate seasonal and spatial variabilities of the LCC. It has a maximum southward component (0.32 m/s), occurring near the surface in winter (Fig. 16 Jan) with a width of 100 km and the depth of 1500 m. The core of the LCC is close to the coast and near the surface. In the spring, it weakens to 0.20 m/s (Fig. 16 Apr), but the width and depth are almost unchanged. It further weakens to a minimum of 0.08 m/s in summer (Fig. 16 Jul) and fall (Fig. 16 Oct). The simulated LCC in spring (Fig. 16 Apr) is qualitatively consistent with a recent geostrophic calculation relative to the sea floor based on CTD measurements. Moreover, there is a very weak (0.01–0.04 m/s) northward return flow on the continental shelf underneath the LCC, with a width of 30 km between 100 and 250 m deep.

7.3. North Korean Cold Current

The NKCC is the continuation of LCC, flowing southward along the Korean coast. To present its seasonal variability, we plot the simulated bi-weekly surface current vectors (Fig. 17) in the southwest JES (127°– 133°E, 35°– 42°N). The NKCC is evident in winter and weakens in summer.

Zonal cross-sections of the meridional velocity at 40°N for January (winter), April (spring), July (summer), and October (fall) indicate seasonal and spatial variabilities of the NKCC. It flows along the continental slope with a maximum southward component (0.1 m/s) in winter and spring. The core of the NKCC is subsurface and close to the shelf break with a width of 100 km and depth of 1500 m (Fig. 18 Jan). The NKCC weakens in summer (Fig. 18 Jul) and fall (Fig. 18 Oct).

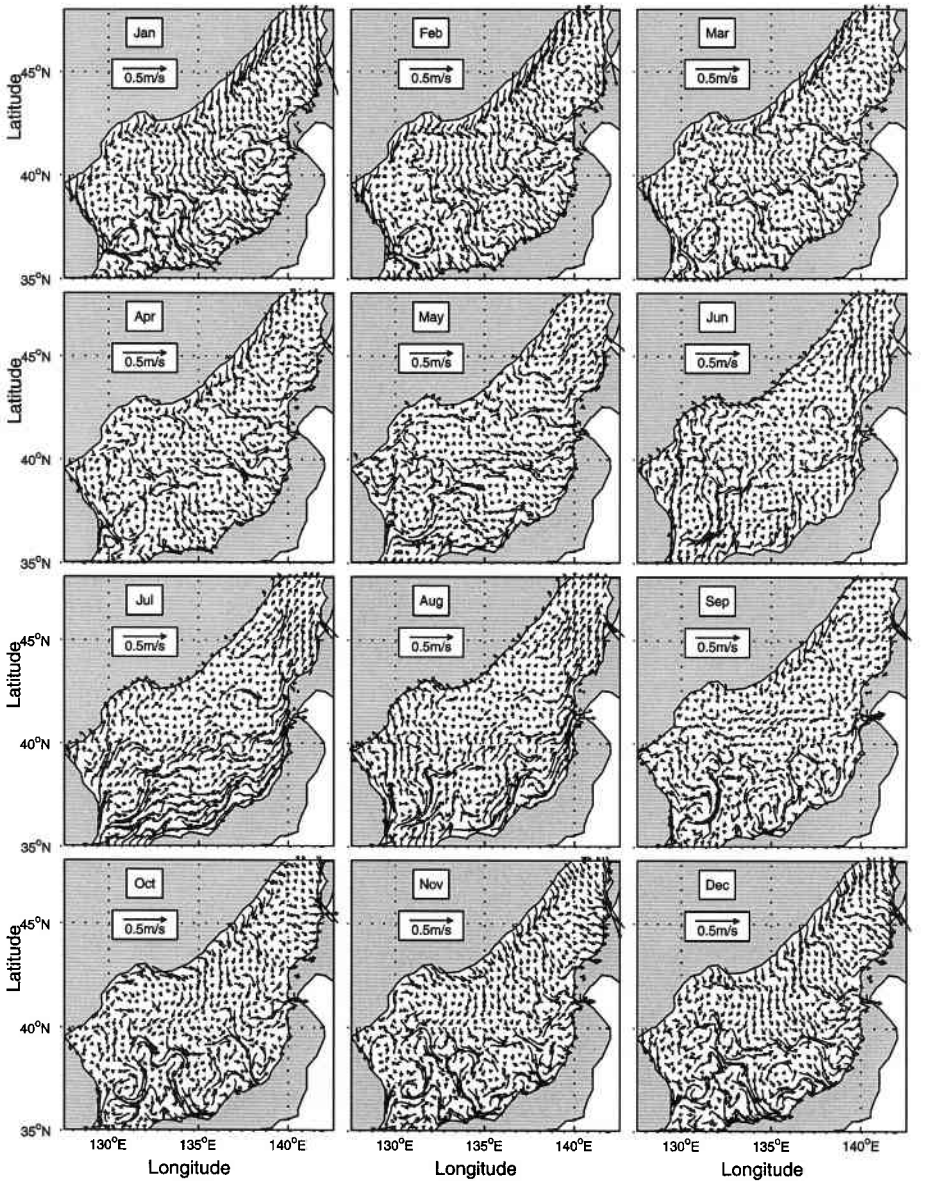

Figure 15. Simulated monthly mean surface velocity vector field.

7.4. Tsushima Warm Current Bifurcation

The TWC enters the JES through the western and eastern channels of the Korea/Tsushima Strait. The simulated bi-weekly velocity vector fields at 10 m depth (Fig. 17) show a branching pattern. This is the result of the boundary specification. The currents through the eastern channel flow along the Japanese coast and form the FBTWC. The flow through the western channel becomes

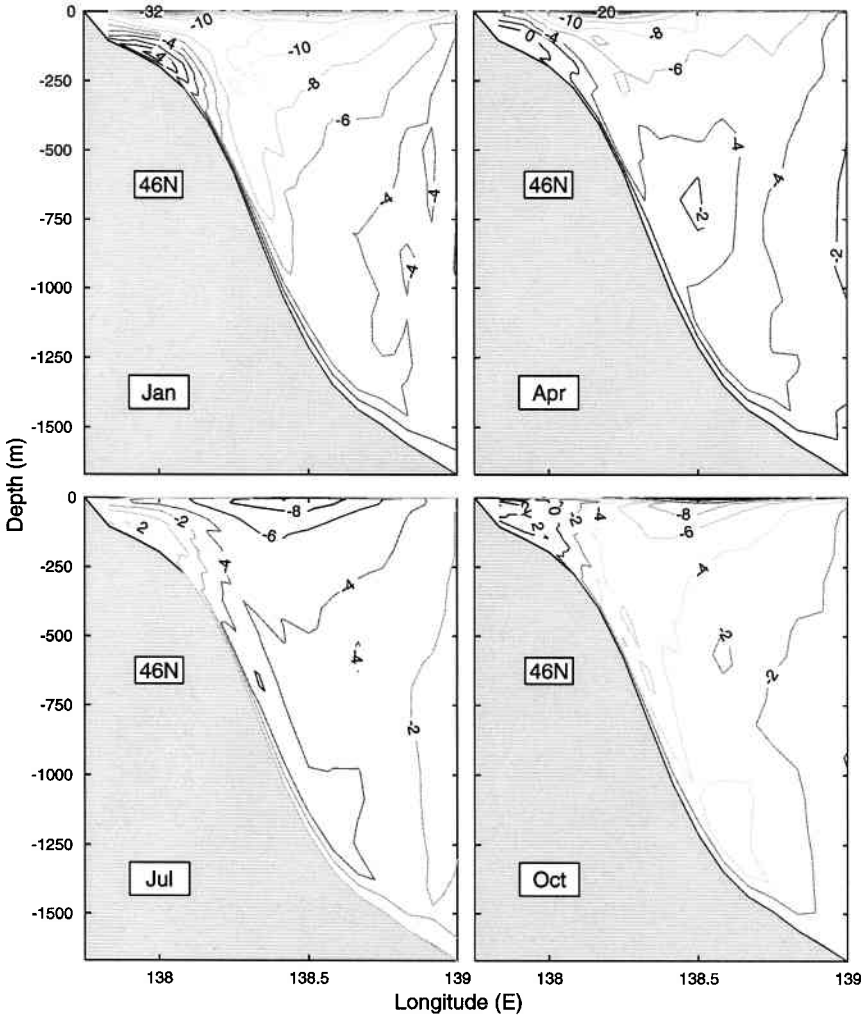

Figure 16. Simulated monthly mean meridional velocity (cm s^{-1}) along 46°N.

the EKWC, which closely follows the Korean coast until it separates near 37°N into northern and eastern branches (first bifurcation). The eastern branch after the first bifurcation flows eastward until 132°E and further separates (second bifurcation) into eastern and northern branches. The eastern branch after the second bifurcation continues to flow eastward and becomes the SBTWC. The northern branch after the second bifurcation flows northward and recirculates near 38°N as the northern flank of a cyclonic eddy located at (130°– 132°E, 36°– 38°N) in the southern UTB.

7.5. Dual Eddies Near Korean Coast

Meanders and eddies are simulated along the four major current systems north of Korea/Tsushima Strait (EKWC, NKCC, FBTWC, and SBTWC): an evident cyclonic eddy in the southern UTB as noted above and an anticyclonic eddy near Korean coast. The southern UTB cyclonic eddy has

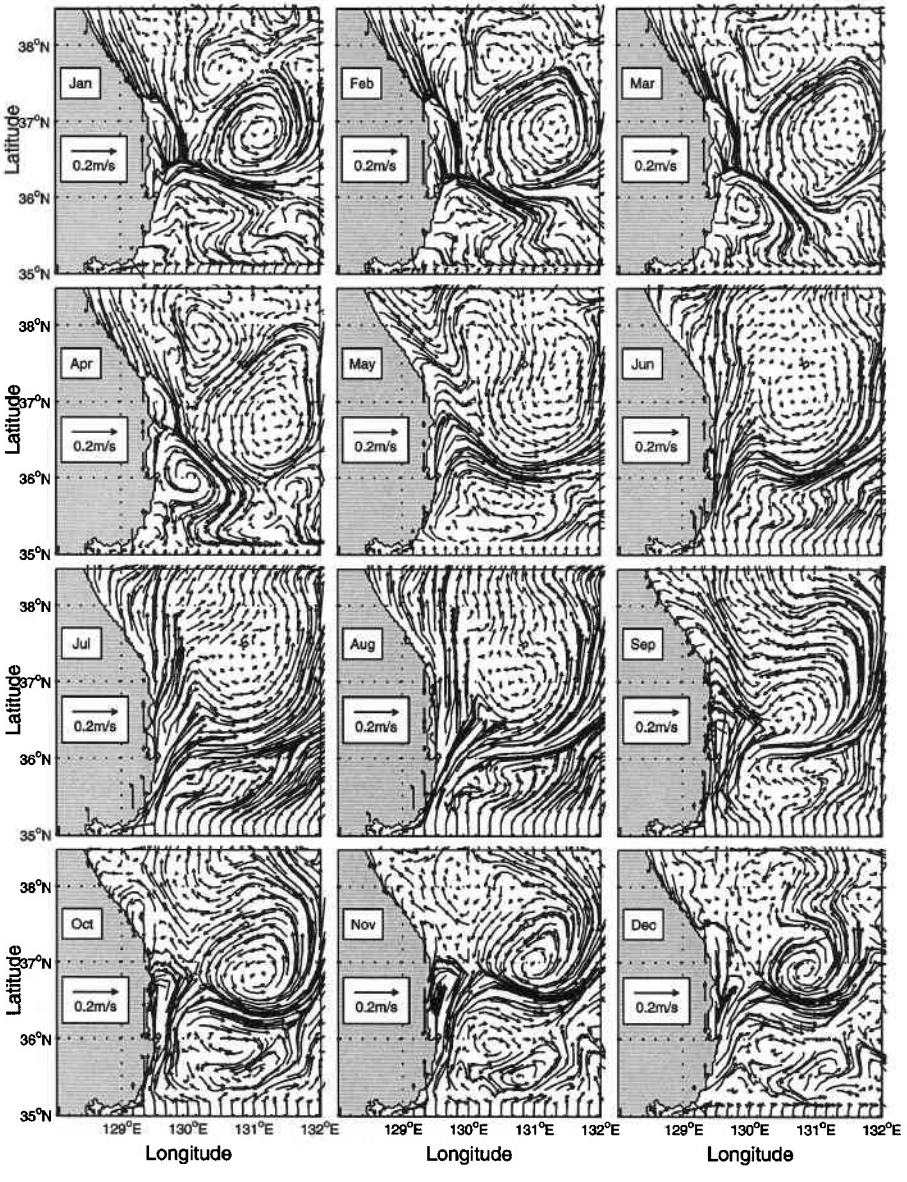

Figure 17. Simulated bi-weekly surface velocity vector field in the Ulleung/Tsushima Basin.

pronounced feature in winter, while the northwestern flank (westward flow) of this eddy weakens throughout summer showing strong EKWC heading toward the interior of the JES.

Such a dipole structure of gyres with an anticyclonic eddy near the Korean coast and a cyclonic eddy in UTB was reported by Shin et al. (1995; 1996) using the data collected from CTD and ADCP measurements in the southwestern JES from March to June 1992.

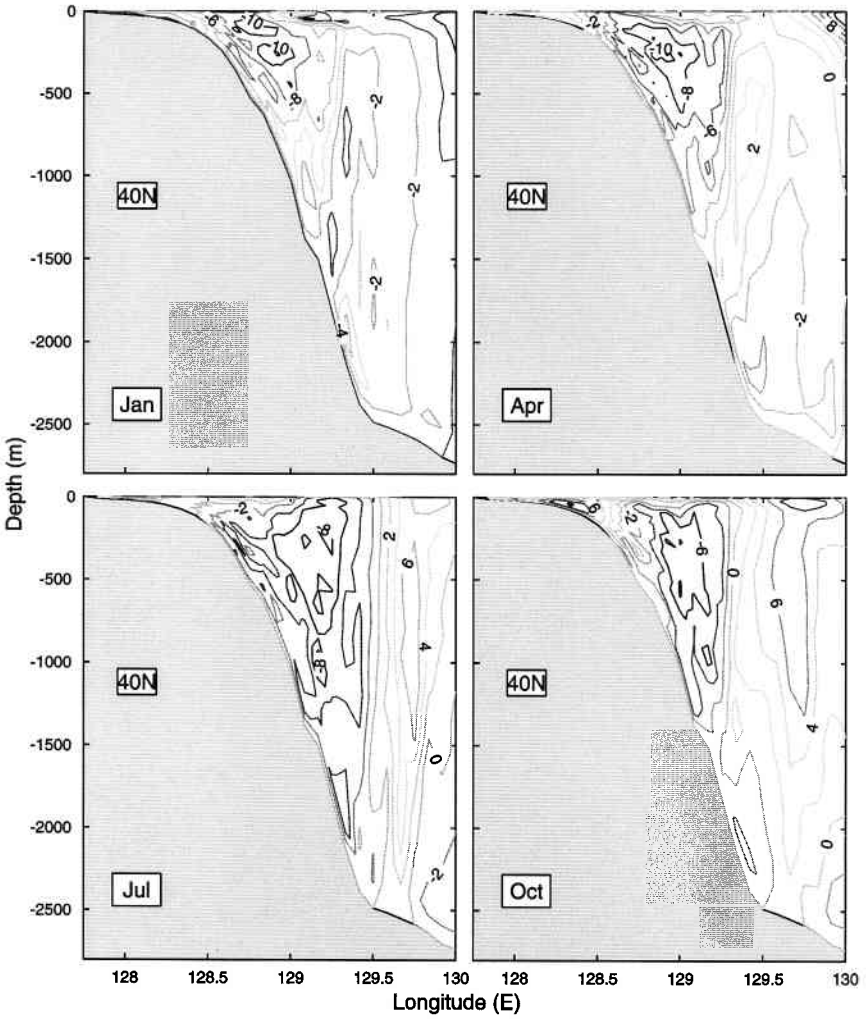

Figure 18. Simulated monthly mean meridional velocity (cm s^{-1}) along 40°N.

7.6. Two Tsushima Warm Current Branches Along the Japanese Coast

The TWC along the Japanese coast is characterized by strong variabilities in connection with many meanders and eddies (Fig. 15). Hase et al. (1999) identified the two main branches of the TWC along the Japanese coast using ADCP and CTD measurements conducted east of Oki Islands every early summer of 1995-1998, and used an analysis of temperature distribution at 100 m depth and the tracks of surface drifters.

The two TWC branches along the Japanese coast are simulated in the model (Fig. 15). To present such a feature more clearly, we plotted the meridional cross-sections of the zonal velocity (Fig. 19) along 135°E for January (winter), April (spring), July (summer), and October (fall). The FBTWC exists throughout the year. It starts from the eastern channel of Korea/Tsushima Strait, flows along the Japanese coast, and flows out of the JES through Tsugaru Strait (Fig. 15). The FBTWC exists

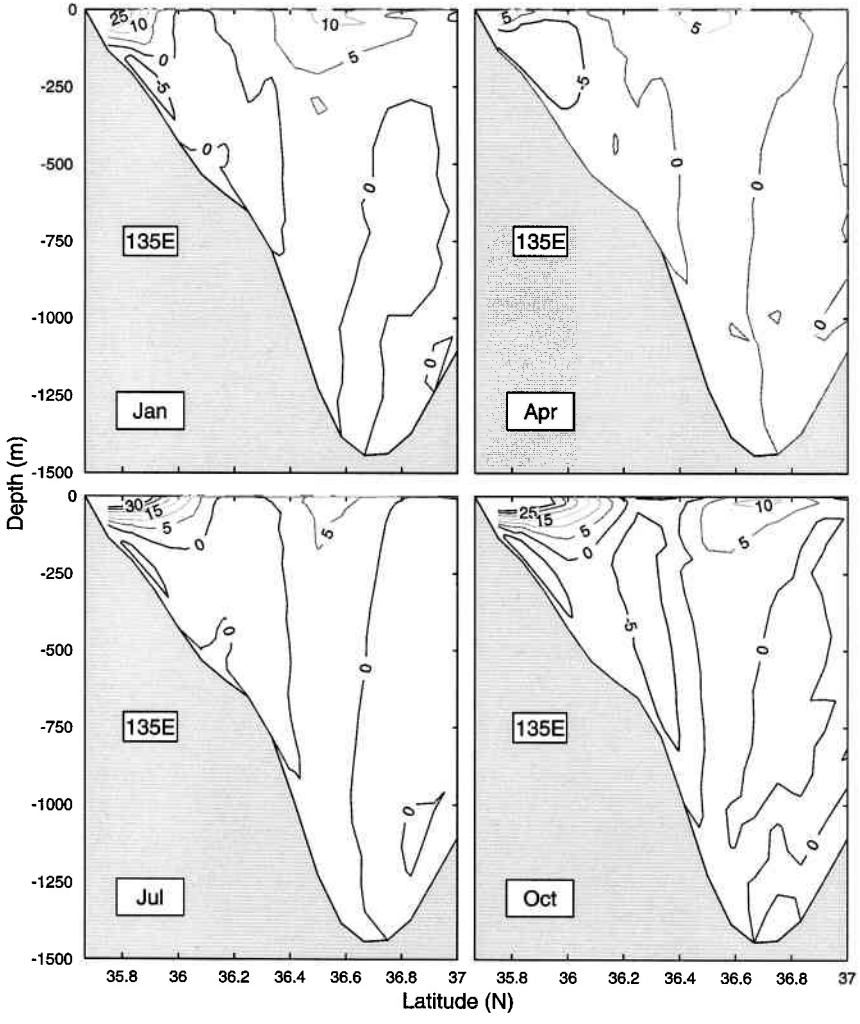

Figure 19. Simulated monthly mean zonal velocity (cm s^{-1}) along 135°E.

throughout the year and flows inshore of the 500 m isobath with a maximum strength (0.3 m/s) and spatial extent (0 to 200 m deep and 50 km wide) in July and October, and a minimum strength (0.1 m/s) and spatial extent (0 to 50 m deep and 20 km wide) in April. The current flowing through the western channel of the Korea/Tsushima Strait feeds the SBTWC, which is weaker than the FBTWC west of the Oki Islands (Fig. 18). The simulated SBTWC also exists throughout the year with a maximum strength (0.1 m/s) in October and January, and a minimum strength (0.05 m/s) in April and July. The simulated TWC branching qualitatively coincides with recent observational studies (Hase et al., 1999). A westward flowing under-current is also simulated below the FBTWC with a speed of 0.05 m/s (Fig. 19), which coincides with Seung and Yoon's (1995) observational study.

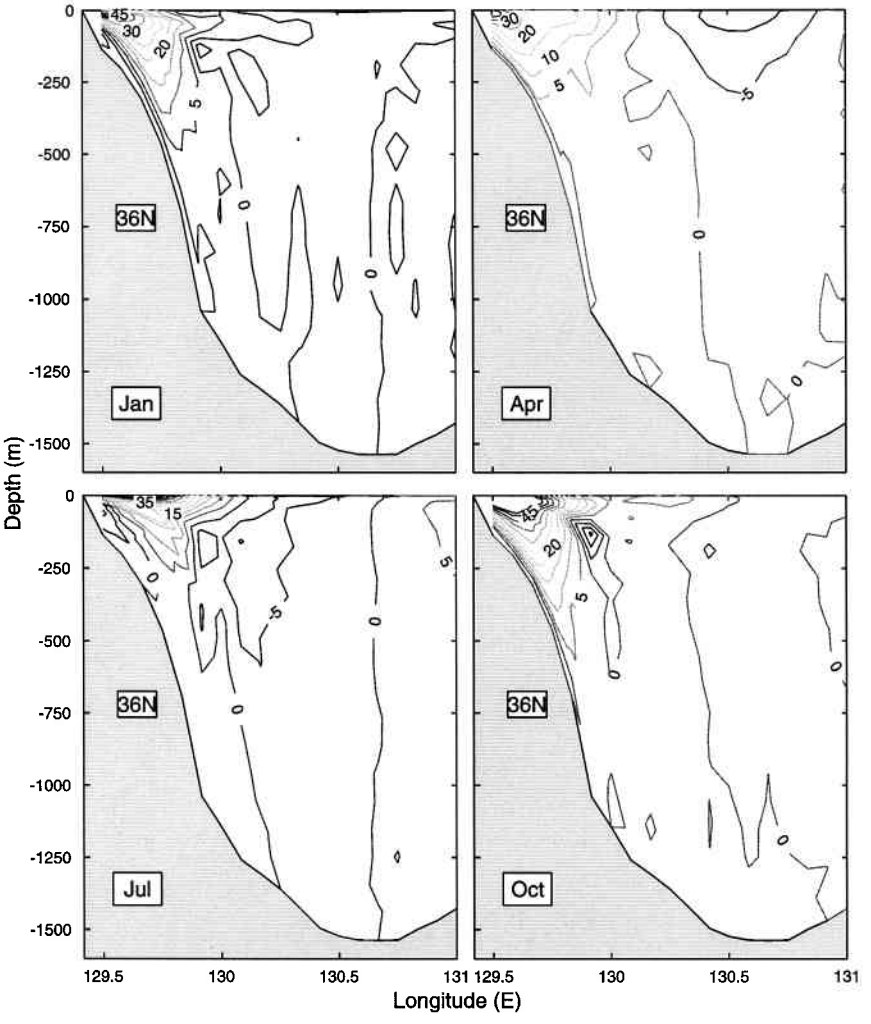

Figure 20. Simulated monthly mean meridional velocity (cm s^{-1}) along 36°N.

7.7. East Korean Warm Current

Zonal cross-sections of the meridional velocity at 36°N for January (winter), April (spring), July (summer), and October (fall) indicate seasonal and spatial variabilities of the EKWC (Fig. 20). It has a maximum northward component (0.65 m/s), occurring near the surface in summer with a width of 80 km and a depth of 200 m. The core of the EKWC is close to the coast and near the surface. In winter, it weakens to a narrow and shallow current with speed of about 0.3 m/s. These features are consistent with local observations off the Korean coast (Shin et al., 1995; 1996). The simulated seasonal variability of EKWC is also consistent with the observational analysis reported by Chu et al. (2001a).

This model simulates the anticyclonic eddy off Korean coast around 38°N during March and April as observed by Shin et al. (1995). The relatively small-scale eddy was found on the inner shelf of

the bifurcation front of the EKWC and KNCC, presumably as consequence of entrainment of south flowing NKCC and a part of northward EKWC.

8. CONCLUSIONS

The JES circulation and thermohaline structure were simulated in this study using POM with seasonal surface flux forcing. Two steps are used to initialize POM. During the first step (restoring run), POM is integrated for two years from zero velocity and January climatological temperature and salinity fields with climatological monthly mean surface wind stress. The final states of the restoring run are taken as initial conditions for the second step (simulation run). During the simulation run, POM is integrated again for two more years with climatological monthly mean surface wind stress, net heat flux, and freshwater flux from the COADS data. The simulated temperature and salinity fields are consistent with observational studies reported by Chu et al. (2001a).

POM simulates the formation of the JES SPF and its seasonal variation. The simulated thermal field shows a strong north-south thermal asymmetry across the SPF. Deeper than 500 m, the temperature is uniformly cold (1–2°C). In winter, the thermocline occurs in the southern JES, and disappears north of 41°N. The strength decreases with latitude from 7°C/100 m near the Japan coast to less than 1°C/100 m at 40°N. In the summer, a strong seasonal thermocline, caused by strong surface heating, is simulated in the shallow depths overlying the permanent thermocline. The seasonal thermocline is sustained from summer to fall.

South of the SPF, the permanent thermocline is located at 80 to 250 m and occurs throughout the year with a maximum strength (0.08°C m^{-1}) in August. Above it, the seasonal thermocline occurs from the surface to 50 m depth in June (0.15°C m^{-1}), intensifies during the summer monsoon season to a maximum value of around 0.36°C m^{-1} in August, and weakens in September. In October, the seasonal thermocline erodes and the ocean mixed layer develops with 50 m near the Korean coast and 130 m near the Japanese coast, a westward uplift of the mixed layer depth. The OML starts to warm at a rate of 2°C/month from March to April, and its depth shoals accordingly. The mixed layer shoaling simulated using POM is a month earlier compared to the observational data.

North of the SPF, the permanent thermocline is quite weak. The seasonal thermocline occurs from the surface to 50 m depth in May ($\sim$ 0.08°C m^{-1}), intensifies during the summer monsoon season to a maximum value of around 0.5°C m^{-1} in August and September, and weakens in October. In November, the seasonal thermocline erodes and becomes part of the permanent thermocline, which weakens during the prevailing winter monsoon season. In February, the permanent thermocline is so weak that the water column is almost uniformly cold (1°C) west of 136°E and weakly stratified ($\leqslant$ 0.01°C m^{-1}) east of 136°E.

POM simulates the surface salinity field reasonably well with surface field characterized by stronger seasonal variability south of the SPF than north of it. The model also simulates a strong north-south salinity asymmetry across the SPF with a salty tongue (> 34.1 ppt) appearing only south of the SPF. The shallow and strong halocline associated with strong thermocline makes the subsurface waters north of the SPF hydrostatically stable. The mid-level salty tongue associated with the weak and thick thermocline makes the water mass hydrostatically less stable south of the SPF.

POM simulates the strong north-south asymmetry of the seasonal halocline with an evident salinity minimum south of the SPF and absence of a salinity minimum north of the SPF. South of the SPF, the SMIN (S < 34.08 ppt) occurs during the summer monsoon season (July-October) underneath a horizontally oriented SMAX with a salty core (S > 34.3 ppt) at 100 m depth. The interface between the SMIN and the SMAX is located at 100 to 200 m depth. During the winter monsoon season, the SMIN is not evident. North of the SPF, the high salinity water (S > 34.05 ppt) of the HSIW appears in the eastern JB (40°– 43°N).

POM simulates the JES circulation reasonably well, especially the Tsushima Current and its bifurcation. The Tsushima Current bifurcates into a western and an eastern branch north of the Korea/Tsushima Strait. The flow through the eastern channel continues along the Japanese coast and forms the first branch of TWC (FBTWC). The flow through the western channel becomes the EKWC, which closely follows the Korean coast until it separates near 37°N into northern and eastern branches (first bifurcation). The eastern branch after the first bifurcation flows eastward until 132°E and further separates (second bifurcation) into eastern and northern branches. The eastern branch after the second bifurcation continues to flow eastward and becomes the second branch of the TWC (SBTWC). The FBTWC exists throughout the year and flows inshore of the 500 m isobath with a maximum strength (0.3 m/s) and spatial extent (0 to 200 m deep and 50 km wide) in July and October, and a minimum strength (0.1 m/s) and spatial extension (0 to 50 m deep and 20 km wide) in April. The simulated SBTWC also exists throughout the year and flows parallel to the continental margin with a maximum strength (0.1 m/s) in October and January, and a minimum strength (0.05 m/s) in April and July.

The other currents such as the LCC, EKWC, and NKCC are simulated reasonably well. The simulated LCC has a maximum southward component (0.32 m/s), occurring near the surface in winter with a width of 100 km and extending to a depth of 800 m. It weakens to a minimum of 0.08 m/s in summer and fall, and shrinks in size to a width of 60 km and depth of 400 m. The simulated EKWC varies from 0.65 m/s (summer) to 0.30 m/s (winter). The EKWC has a width of 80 to 100 km and a depth of about 200 m throughout the year. The northward branch (overshoot) of EKWC leaves the Korean coast and converges with the southward flowing NKCC, and forms a current meandering eastward along the SPF. The simulated NKCC flows along the continental slope with a maximum southward component (0.1 m/s) in winter and spring. The core of the NKCC is close to the shelf break with a width of 100 km and depth of 1500 m.

Using realistic bottom topography, POM successfully simulates the dipole structure of gyres in the southern JES with an anticyclonic eddy near the Korean coast and a cyclonic eddy in UTB as reported by Shin et al. (1995; 1996). The southern UTB cyclonic eddy has a pronounced feature in winter, while the northwestern flank (westward flow) of this eddy weakens throughout summer showing strong EKWC heading toward the interior of the JES.

Although POM adequately simulated the seasonal JES circulation and thermohaline structure, much more modeling work is required. Three-dimensional observations of ocean temperature, salinity and velocity fields would allow initialization of the model with a more realistic dynamic and thermodynamic structure. Atmospheric forcing could also be made more realistic by utilizing a coupled Ocean/Atmosphere model, such as the Coupled Atmosphere and Ocean Coastal System (CAOCS) under development by the Naval Postgraduate School (Chu et al., 1999a). Use of such a system would provide more accurate wind stress forcing, through modifications of the wind field by surface frictional effects, inclusion of ocean wave effects, and improved ocean/atmosphere thermal and salinity fluxes.

Future studies should concentrate on less simplistic scenarios. Realistic inflow transport should be included, and the use of interpolated climatological winds needs to be upgraded to incorporate synoptic winds to improve realism.

ACKNOWLEDGMENTS

The authors wish to thank George Mellor and Tal Ezer of the Princeton University for most kindly providing us with a copy of POM code and Yuchun Chen for programming assistance. We deeply thank Christopher N.K. Mooers of the University of Miami and an anonymous reviewer for their critiques, which significantly improved this chapter. This work was funded by the Office of Naval

Research, the Naval Oceanographic Office, and the Naval Postgraduate School. Financial support to Chang S. Kim through the DUT program by the Ministry of Science and Technology Korea is appreciated.

REFERENCES

Bang, I., Choi, J.-K., Kantha, C., Horton, C., Cliford, M., Suk, M-S., Chang, K-I., Nam, S.Y., Lie, H-J., 1996. A hindcast experiment in the East Sea (Sea of Japan). La Mer, 34: 108–130.

Blumberg, A., and Mellor, G., 1987. A description of a three dimensional coastal ocean circulation model. In: Heaps, N.S. (Editor), Three-Dimensional Coastal Ocean Models, pp. 1–16. Washington, DC: American Geophysics Union.

Chu, P.C., 1995. P-vector method for determining absolute velocity from hydrographic data. Marine Technology Society Journal, 29 (3): 3–14.

Chu, P.C., Chen, Y.C., and Lu, S.H., 1998. Temporal and spatial variabilities of Japan Sea surface temperature and atmospheric forcings. Journal of Oceanography, 54: 273–284.

Chu P. C., Chen, Y., and Lu, S.,1999a. Japan/East Sea (JES). Subpolar front meandering and eddy shedding in May 1995. Proceedings of the CREAMS'99 International Symposium, Fukuoka, Japan, pp. 11–13.

Chu, P.C., Lan, J., and Fan, C.W., 2001a. Japan Sea thermohaline structure and circulation, Part 1. Climatology. Journal of Physical Oceanography, 31: 244–271.

Chu, P.C., Lan, J., and Fan, C.W., 2001b. Japan Sea thermohaline structure and circulation, Part 2. A variational P-vector method. Journal of Physical Oceanography, 31: 2886–2902.

Chu, P.C., Lan, J., and Strauhs, H., 2000. A numerical simulation of Japan/East Sea (JES) seasonal circulation. In: Spaulding, M.L., and Butler, H.L. (Editor), Estuarine and Coastal Modeling, pp. 94–113. New York: American Society of Civil Engineers.

Chu, P.C., Lu, S.H., and Chen, Y.C., 1999b. Circulation and thermohaline structures of the Japan/East Sea (JES) and adjacent seas simulated by a nested basin/coastal model. Proceedings of the CREAMS'99 International Symposium, Fukuoka, Japan, pp. 108–111.

Chu, P.C., Wang, G.H., and Chen, Y.C., 2002. Japan Sea thermohaline structure and circulation, Part 3. Autocorrelation functions. Journal of Physical Oceanography, 32: 3596–3615.

da Silva, A.M., Young, C.C., and Levitus, S., 1994. Atlas of Surface Marine Data 1994. Technical Report Geoscience, 94. Milwaukee, WI: University of Wisconsin-Milwaukee, 83p.

Gong, Y., and Park, C.G., 1969. On the oceanographical character of the low temperature region in the eastern sea of Korea. Bulletin Fisheries Research Development Agency, Korea, 4: 69–91.

Haney, L.R., 1971. Surface boundary condition for ocean circulation models. Journal of Physical Oceanography, 1: 241–248.

Hase, H., Yoon, J.-H., and Koterayama, W., 1999. The branching of the Tsushima Warm Current along the Japanese coast. Proceedings of the CREAMS'99 International Symposium, Fukuoka, Japan, pp. 19-22.

Hirose, N., Kim, C.H., and Yoon, J.H., 1996. Heat budget in the Japan Sea. Journal of Oceanography, Society of Japan, 52: 553–574.

Hogan, P.J., and Hurlburt, H.E., 1999a. A possible mechanism for the formation of the boundary current along the coast of Honshu in Japan/East Sea. Proceedings of the 10th PAMS/JECSS Workshop, Kagoshima, Japan, pp. 6.8–6.11.

Hogan, P.J., and Hurlburt, H.E., 1999b. Impact of different wind forcing on Japan/East Sea circulation. Proceedings of the CREAMS'99 International Symposium, Fukuoka, Japan, pp. 124–127.

Hogan, P.J., and Hurlburt, H.E., 2000a. Impact of upper ocean topographical coupling and isopycnal outcropping in Japan/East Sea models with 1/8 to 1/64 resolution. Journal of Physical Oceanography, 30: 2535–2561.

Hogan, P.J., and Hurlburt, H.E., 2000b. Modeled surface circulation in the Japan/East Sea: Impact of using different climatological wind forcing sets. Proceedings of the International Conference on Coastal Ocean and Semi-Enclosed Seas: Circulation and Ecology Modeling and Monitoring, Moscow, Russia, pp. 57-60.

Holloway, G., Sou, T., and Eby, M., 1995. Dynamics of circulation of the Japan Sea. Journal of Marine Research, 53: 539–569.

Isoda, Y., and Saitoh, S., 1993. The northward intruding eddy along the east coast of Korea. Journal of Oceanography, 17: 265–276.

Isoda, Y., Saitoh, S., and Mihara, M., 1991. SST structure of the Polar Front in the Japan Sea. In: Yakano, K. (Editor), Oceanography of Asian Marginal Seas, pp. 103–112. Amsterdam, The Netherlands: Elsevier Science.

Kawabe, M., 1982a. Branching of the Tsushima Current in the Japan Sea, Part I. Data analysis. Journal of Oceanographical Society of Japan, 38: 95–107.

Kawabe, M., 1982b. Branching of the Tsushima Current in the Japan Sea, Part II. Numerical experiment. Journal of Oceanographical Society of Japan, 38: 183–192.

Kim, K., and Chung, J.Y., 1984. On the salinity-minimum layer and dissolved oxygen-maximum layer in the East Sea (Japan Sea). In: Ichiye, T. (Editor), Ocean Hydrodynamics of the Japan and East China Sea, pp. 55–65. Amsterdam, The Netherlands: Elsevier Science.

Kim, Y.G., and Kim, K.K., 1999. Intermediate waters in the East/Japan Sea. Journal of Oceanography, 55: 123–231.

Kim, C.-H., and Yoon, J.-H.,1994. A numerical study on the seasonal variation of the Tsushima Warm Current along the coast of Japan. Proceedings of the CREAMS Third Workshop. Seoul, Korea, pp. 73–79.

Kim, C.-H., and Yoon, J.-H., 1996. Modeling of the wind-driven circulation in the Japan Sea using a reduced gravity model. Journal of Oceanography, 52: 359–373.

Kim, C.-H., and Yoon, J.-H., 1999. A numerical modeling of the upper and the intermediate layer circulation in the East Sea. Journal of Oceanography, 55: 327–345.

Levitus, S., 1982. Climatological atlas of the World Ocean. NOAA Professional Paper 13. Washington DC: National Ocean and Atmospheric Administration.

Maizuru Marine Observatory, 1997. Bulletin of the Maizuru Marine Observatory.

Martin, S., and Kawase, M., 1998. The southern flux of sea ice in the Tatarskiy Strait, Japan Sea and the generation of the Liman Current. Journal of Marine Research, 56: 141–155.

Miyazaki, M., 1952. The heat budget of the Japan Sea. Bulletin of Hokkaido Reg. Fisheries Research Laboratory, 4: 1–54 (in Japanese with English abstract).

Miyazaki, M., 1953. On the water masses of the Japan Sea. Bulletin of Hokkaido Reg. Fisheries Research Laboratory, 7: 1–65 (in Japanese with English abstract).

Mooers, C. N.K., and Kang, H.-S., 1995. Initial spin-up of a Sea of Japan numerical circulation model. In: Alekseev, A.S., and Bakhvalov, N.S. (Editors), Advanced Mathematics: Computations and Applications, pp. 350–357. Novosibirsk: NCC Publisher.

Moriyasu, S., 1972. The Tsushima Current. In: Stommel, H., and Yoshida, K. (Editors), Kuroshio-Its Physical Aspects, pp. 353–369. Tokyo: University of Tokyo Press.

Na, J.-Y., Seo, J.-W., and Han, S.-K., 1992. Monthly mean sea surface winds over the adjacent seas of the Korean Peninsula. Journal of Oceanology Society Korea, 27: 1–10.

Preller, R.H., and Hogan, P.J., 1998. Oceanography of the Sea of Okhotsk and the Japan/East Seas. In: Robinson, A.R., and Brink, K.K. (Editors), The Sea, pp. 429–481. New York: John Wiley and Sons, Inc.

Sekine, Y., 1991. Wind-driven circulation in the Japan Sea and its influence on the branching of the Tsushima Current. Progress in Oceanography, 17: 297–312.

Senjyu, T., 1999. The Japan Sea Intermediate Water: its characteristics and circulation. Journal of Oceanography, 55: 111–122.

Seo, J. W., 1998. Research on the sea surface winds and heat flux in the East Asian Marginal Seas. Ph.D. Thesis. China: Hanyang University.

Seung, Y.H., 1992. A simple model for separation of East Korean Warm Current and formation of the North Korean Cold Current. Journal of Oceanology Society Korea, 27: 189–196.

Seung, Y.H., and Kim, K., 1989. On the possible role of local thermal forcing on the Japan Sea circulation. Journal of Oceanology Society Korea, 24: 1–14.

Seung, Y.H., and Kim, K., 1993. A numerical modeling of the East Sea circulation. Journal of Oceanology Society Korea, 28: 292–304.

Seung, Y.H., and Kim, K.J., 1995. A multilayer model for dynamics of upper and intermediate layer circulation of the East Sea. Journal of Oceanology Society Korea, 30: 227–236.

Seung, Y.H., and Nam, S.Y., 1992. A numerical study on the barotropic transport of the Tsushima Warm Current. La Mer, 30: 139–147.

Seung, Y.H., and Yoon, J.-H., 1995. Some features of winter convection in the Japan Sea. Journal of Oceanography, 51: 61–73.

Shin, H.-R., Byun, S.-K., and Kim, C., 1995. The characteristics of structure of warm eddy observed to the northwest of Ulleungdo in 1992. Journal of Oceanology Society Korea, 30: 39–56 (in Korean with English abstract).

Shin, C.W., Byun, S.K., and Kim, C.S., 1996. Comparison between geostrophic currents in the southwestern part of the East Sea. Journal of Oceanology Society Korea, 31: 89–96.

Smagorinsky, J., 1963. General circulation experiments with the primitive equations, I. The basic experiment. Monthly Weather Review, 91: 99–164.

Toba, Y., Tomizawa, K., Kurasawa, Y., and Hanawa, K., 1982. Seasonal and year-to-year variability of the Tsushima-Tsugaru Warm Current system with its possible cause. La Mer, 20: 41–51.

Uda, M., 1934. The results of simultaneous oceanographic investigations in the Japan Sea and its adjacent waters in May and June. Journal Imp. Fish. Exp. Sta., 5: 57–190 (in Japanese).

Yi, S.U., 1966. Seasonal and secular variations of the water volume transport across the Korea Strait. Journal of Oceanography Society Korea, 1: 7–13.

Yoon, J.-H., 1982a. Numerical experiment on the circulation in the Japan Sea, Part I. Formation of the East Korean Warm Current. Journal of Oceanography Society Japan, 38: 43–51.

Yoon, J.-H., 1982b. Numerical experiment on the circulation in the Japan Sea, Part II. Influence of seasonal variations in atmospheric conditions on the Tsushima Current. Journal of Oceanography Society Japan, 38: 81–94.

Yoon, J.-H., 1982c. Numerical experiment on the circulation in the Japan Sea Part, III. Mechanism of the nearshore branch of the Tsushima Current. Journal Oceanography Society Japan, 38: 125–130.

Yoshikawa, Y., Awaji, T., and Akitomo, K., 1999. Formation and circulation processes of intermediate water in the Japan Sea. Journal of Physical Oceanography, 29: 1701–1722.